Static and Dynamic Stereochemistry and Solvation of 2,2-Ditipylethenols[1]

Joseph Frey and Zvi Rappoport*

Department of Organic Chemistry and the Minerva Center for Computational Quantum Chemistry, The Hebrew University, Jerusalem 91904, Israel

Received June 11, 1997[⊗]

The effect of increased bulk of the β-aryl group in enols $Ar_2C{=}C(OH)R$ from Ar = mesityl = Mes (**1**) to Ar = 2,4,6-*i*-$Pr_3C_6H_2$ = Tip (**2**) was investigated. The solid-state structure when R = H (**a**) does not significantly differ for **1a** and **2a**. The dynamic behavior of **2a** resembles that of **1a**, but the rotational barriers for both the threshold one-ring flip process and the two-ring flip process are higher for **2a**. The one-ring flip barrier for **2a** is solvent-dependent. The threshold two-ring flip barriers when R = Me (**2b**) and *t*-Bu (**2c**) are higher than for the mesityl analogues, but that for **2c** is higher than predicted. Solvations of **2a** and **1a** and their associations with DMSO are similar. The C=COH conformation is *syn*-planar with an OH···π(Tip) association in non-hydrogen-bond-accepting solvents and is *anti*-clinal with OH···solvent association in hydrogen-bond-accepting solvents. In summary, the increased bulk associated with the change Mes → Tip changes the structure and behavior in the expected direction but, except for the $\Delta G_c^{\ddagger}$ values, not to a large extent.

2,2-Dimesityl-1-R-ethenols (**1**) are stable enols whose structures were proven by chemical, spectroscopic, and crystallographic methods.[2] They exist in enantiomeric vinyl propeller conformations differing in their helicities. Their static and dynamic behaviors were extensively investigated[2] and recently reviewed.[3] X-ray diffractions corroborated the proposed propeller conformations,[4] and molecular mechanics (MM) computations confirmed that they are actual energy minima.[5]

In analogy with Mislow's analysis[6] the correlated helicity reversal rotation of the aryl rings can be conveniently analyzed in terms of "flip" mechanisms. The ring that "flips" passes through a plane perpendicular to the ideal double bond plane while the remaining ("nonflipping") ring(s) rotate concurrently and disrotatorily and pass through the double-bond plane. The number of flipping rings designates the different flip mechanisms as zero-, one-, or two-ring flip;[7] e.g., if both the β and β' rings pass through the normal to the ideal double-bond plane, the pathway is designated [β,β']-two-ring flip (vide infra). A rotation pathway not resulting in helicity reversal involves a 180° rotation of one or more rings. The threshold rotational enantiomerization mechanism involves a correlated rotation around the C(sp^2)−C(Ar) bond.[8] It is a one-ring flip for **1a** and a two-ring flip for **1b**−**1e**,[9] and the two-ring flip barriers decrease with the increased bulk of R from 14.2 kcal mol^{-1} for R = H (**1a**) to 10.4 kcal mol^{-1} for R = *t*-Bu (**1e**). Similar behavior occurs with the tetra-*m*-Me and tetra-*m*-Br derivatives,[10] and it was ascribed in all systems to steric effects. A vicinal in-plane H/Mes (R/Mes) interaction is lower (larger) than the perpendicular one in the rotational transition state when R (= alkyl, silyl) is bulkier than H. Increased bulk of R increases the Mes−C=C torsional angles and the ground-state energy and lowers the rotational barrier. The proposed enantiomerization mechanism is also supported by a structural correlation analysis[11] of molecules $Ar^1Ar^2C{=}CR^1R$.[4b]

$Mes_2C{=}C(OH)R$

1a: R = H

b: R = Me

c: R = Et

d: R = *i*-Pr

e: R = *t*-Bu

f: R = Mes

Mes = mesityl

The preferred solution conformation was determined primarily by NMR methods under slow exchange, when separate signals for each hydrogen and carbon in the molecule were displayed in the ^1H and ^{13}C NMR spectra.[5,8] The chiral propeller conformation is supported by the NMR spectra of **1d** or of the isopropyl ether $Mes_2C{=}CHOPr\text{-}i$[5] where the *i*-Pr group serves as a

[⊗] Abstract published in *Advance ACS Abstracts,* November 1, 1997.

(1) Presented in part at the 57th Meeting of the Israel Chemical Society, Haifa, Feb 12−13, 1992, Abstract L-32 and at the 11th IUPAC Conference on Physical Organic Chemistry, Ithaca College, Aug 2−7, 1992, Abstract C-13.

(2) For reviews up to 1990 see: (a) Rappoport, Z.; Biali, S. E. *Acc. Chem. Res.* **1988**, *21*, 442. (b) Hart, H.; Rappoport, Z.; Biali, S. E. In *The Chemistry of Enols*; Rappoport, Z. Ed. 1990, Chapter 8, pp 481−590.

(3) Rappoport, Z.; Biali, S. E. *Acc. Chem. Res* **1997**, *30*, 307.

(4) Kaftory, M.; Nugiel, D. A.; Biali, S. E.; Rappoport, Z. *J. Am. Chem. Soc.* **1989**, *111*, 8181.

(5) Biali, S. E.; Nugiel, D. A.; Rappoport, Z. *J. Am. Chem. Soc.* **1989**, *111*, 846.

(6) Mislow, K. *Acc. Chem. Res.* **1976** , *9*, 26.

(7) (a) Kurland, R. J.; Schuster, I. I.; Colter, A. K. *J. Am. Chem. Soc.* **1965**, *87*, 2279. (b) Gust, D.; Mislow, K. *J. Am. Chem. Soc.* **1973**, *95*, 1535.

(8) Biali, S. E.; Rappoport, Z. *J. Am. Chem. Soc.* **1984**, *106*, 477.

(9) (a) Nugiel, D. A.; Biali, S. E.; Rappoport, Z. *J. Am. Chem. Soc.* **1984**, *106*, 3357. (b) Nugiel, D. A.; Rappoport, Z. *J. Am. Chem. Soc.* **1985**, *107*, 3669.

(10) Eventova, I.; Nadler, E. B.; Rochlin, E.; Frey, J.; Rappoport, Z. *J. Am. Chem. Soc.* **1993**, *115*, 1290.

(11) Bürgi, H.-B.; Dunitz, J. D. *Acc. Chem. Res.* **1983**, *16*, 153.

S0022-3263(97)01049-9 CCC: $14.00

Scheme 1

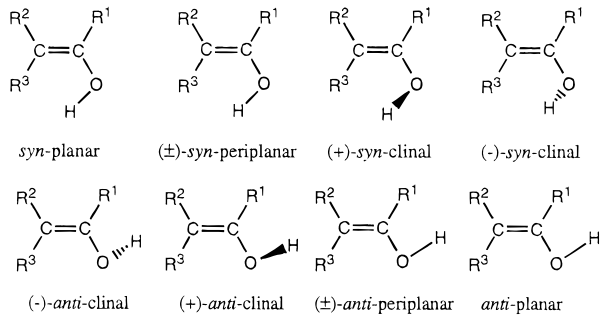

prochiral "chiral probe", and at slow exchange separate signals are displayed for the diastereotopic *i*-Pr methyls.

The preferred C=COH conformations of enols **1** in solution were deduced from NMR and IR data.[12] Eight types of conformations exist that differ in the value of the dihedral angle θ of the C=COH moiety (Scheme 1): two planar, two periplanar (deviating from planarity up to 30°), and four "gauche"-type forms that belong to two pairs of cisoid and transoid nonplanar "clinal" conformers.

^{1}H NMR spectra of **1a**−**g** in various solvents show a strong solvent dependence of δ(OH)[12] and also of $^3J_{HCOH}$ for **1a**.[12] The preferred C=CHOH conformation of **1a** was determined by using the Frazer equation,[13] which relates the $^3J_{HCOH}$ values to the H−C−O−H dihedral angle. In poor hydrogen-bond-accepting solvents, e.g., CCl_4, the C=C−O−H moiety is almost syn planar. The IR spectra of **1a** in CCl_4 indicate the presence of two different species. It was suggested that in the major one the OH group is intramolecularly hydrogen bonded to the π system of the mesityl ring cis to it.[12a] In good hydrogen-bond-accepting solvents (e.g., DMSO), the C=COH conformation is *anti*-clinal in which the OH group is hydrogen bonded to one solvent molecule. From the linear correlation between δ(OH)[**1a**] and those of other enols in the same solvents, similar conformations were assumed for other enols **1**.

Both δ(OH) and $^3J_{HCOH}$ strongly depend on the DMSO-d_6 molar fraction in CCl_4−DMSO-d_6 mixtures.[12] Analysis of the equilibrium between an internally hydrogen-bonded species and a conformer intermolecularly hydrogen-bonded to the solvent gave enol·DMSO association constants.

This hydrogen-bonding effect is supported by X-ray diffraction data.[14] The conformation of **2b**·EtOH is *anti*-periplanar due to hydrogen bonding to the cocrystallized EtOH molecule,[4] whereas enols **1a**,[4] MesC(Ph)=CHOH,[14] and $(Br_2Mes)_2C$=CHOH[10] crystallize as hydrogen-bonded tetramers.

The remarkable stability, the chemical properties, the static and dynamic stereochemistry, and the OH conformation of the crowded mesityl-substituted enols result from the steric bulk and conjugation ability of the mesityl groups. However, whereas the effect of α-R's on these phenomena was extensively investigated, the effect of β-substituents was only slightly investigated. When the hydrogens of the two mesityl groups of **1a**, **1b**, and **1e** were substituted by two *m*-Me or *m*-Br groups the buttressing effect on the conformation and rotational behavior was not large.[10] Consequently, a larger change in the bulk of the β-aryl group is required for observing a significant change. Since no substrate carrying geminal 2,4,6-*t*-$Bu_3C_6H_2$ (supermesityl)[15] groups on carbon is known, a 2,2-ditipyl (tipyl = Tip = 2,4,6-triisopropylphenyl) derivative seems an attractive system.

The stabilities of 2,2-diarylethenols toward ketonization and oxidation increased by replacing the mesityl by tipyl groups. This is ascribed to an "increased [steric] hindrance" by the bulkier tipyl relative to mesityl.[16]

The tipyl (or 2,6-*i*-$Pr_2C_6H_3$) group acts in stereodynamic studies both as a bulky substituent and as a chirality probe. In the chiral conformation where the plane bisecting the Me−CH−Me angle is not the symmetry molecular plane, the two *i*-Pr-methyls are diastereotopic and display anisochronous ^{1}H or ^{13}C NMR signals.[17] A higher enantiomerization barrier ($\Delta G_c^{\ddagger}$) for 2-tipylacenaphthenone compared with the mesityl analogue indicates that the former is more sterically congested in the ground state.[18]

In ketones TipCOR, the Tip-C=O rotational barriers increase with the increased bulk of the R, from 12 kcal mol^{-1} for R = Me to 24 kcal mol^{-1} for R = *t*-Bu. The barriers were higher than for the corresponding MesCOR analogues,[19] thus reflecting the larger steric interaction between the alkyl R and the *o*-*i*-Pr (vs *o*-Me) in the transition state. In ketones $TipCOC_6H_4X$-*p* $\Delta G_c^{\ddagger}$ correlates linearly with σ_X^+ values due to the effect of the conformational change during the Ar−C=O rotation on the ARCO/X resonance interaction.[20]

Akkerman and Coops studied the racemization of diarylacetic acids $(3\text{-Me-}2,4,6\text{-}R_3C_6H)_2CHCOOH$.[21] Optically active acids could not be obtained when R = Me, Et, but for R = *i*-Pr, measurement of the racemization rate was possible, showing again a higher rotational barrier for the Tip than for the Mes derivative.

2,2-Ditipylethenols **2a**−**c** were therefore prepared in order to investigate how the β-Mes → β-Tip change affects (a) the ground-state conformation, (b) the threshold rotational barrier, and (c) the values of the barriers and their order as a function of the α-substituent.

Tip_2C=C(OH)R

2a: R = H

b: R = Me

c: R = *t*-Bu

Results and Discussion

Synthesis of the Enols. Enol **2a** was prepared by Fuson and co-workers by the acid-catalyzed pinacol

(12) (a) Biali, S. E.; Rappoport, Z. *J. Am. Chem. Soc.* **1984**, *106*, 5641. (b) Rappoport, Z.; Nugiel, D. A.; Biali, S. E. *J. Org. Chem.* **1988**, *53*, 4814. (c) Nadler, E. B.; Rappoport, Z. *J. Am. Chem. Soc.* **1989**, *111*, 213.

(13) Fraser, R. R.; Kaufman, M.; Morand, P.; Govil, G. *Can. J. Chem.* **1969**, *47*, 403.

(14) Nadler, E. B.; Röck, M.; Schmittel, M.; Rappoport, Z. *J. Phys. Org. Chem.* **1993**, *6*, 233.

(15) Weidenbuch, M.; Schaefers, K.; Pohl, S.; Saak, W. *J. Organomet. Chem.* **1988**, *346*, 171.

(16) Fuson, R. C.; Chadwick, D. H.; Ward, M. L. *J. Am. Chem. Soc.* **1946**, *68*, 389.

(17) Mislow, K.; Raban, M. *Top. Stereochem.* **1967**, *1*, 1.

(18) Miller, A. R. *J. Org. Chem.* **1976**, *41*, 3599.

(19) Casarini, D.; Lunazzi, L.; Verbeck, R. *Tetrahedron* **1996**, *52*, 2471.

(20) Ito, T.; Umehara Y.; Nakamura, K.; Yamada, Y.; Matsuura, T.; Imashiro, F. *J. Org. Chem.* **1981**, *46*, 4359.

(21) (a) Akkerman, O. S.: Coops, J. *Recl. Trav. Chim. Pays-Bas* **1967**, *86*, 755. (b) Akkerman, O. S. *Recl. Trav. Chim. Pays-Bas* **1970**, *89*, 673.

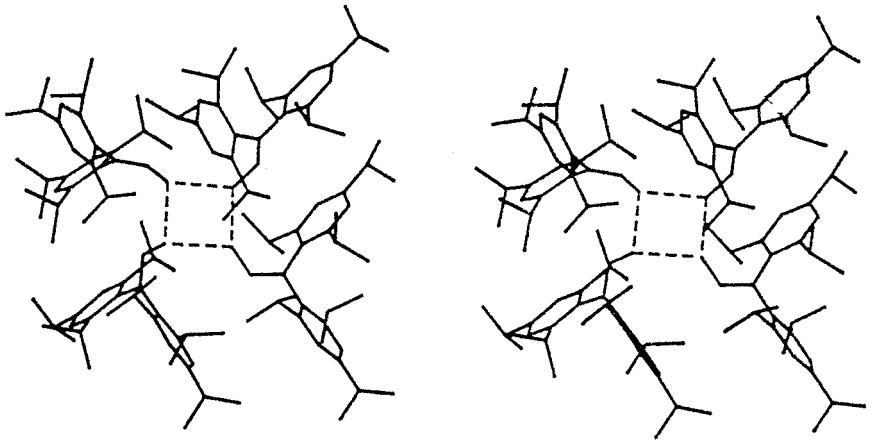

Figure 1. Tetramer hydrogen-bonded arrangement of **2a** held by hydrogen bonds.

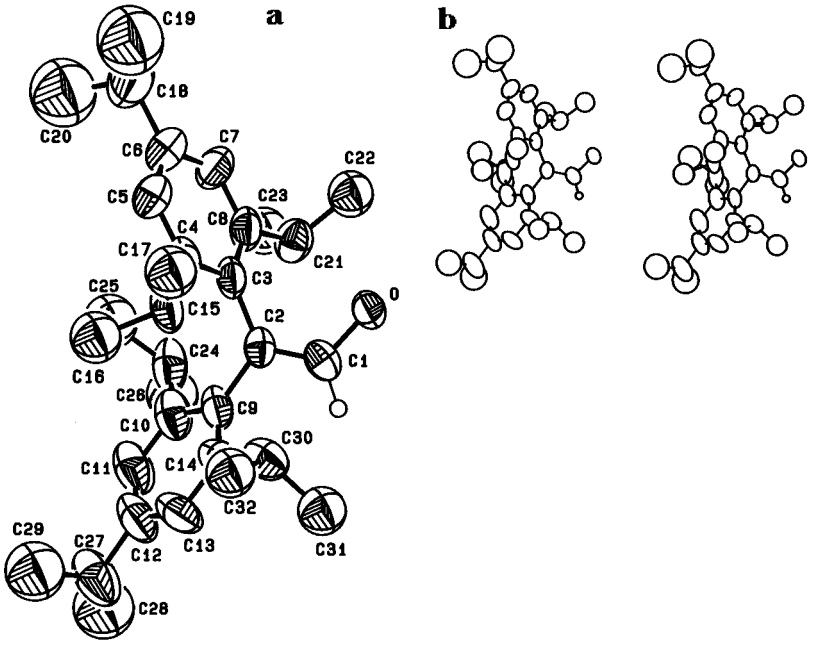

Figure 2. ORTEP drawing and numbering scheme (a) and stereoview (b) of one of the structures of **2a**.

rearrangement of 1,2-ditipylethanediol.[16] It is interesting that a stable enol is apparently thermodynamically more stable than the diol precursor. We prepared **2a** by this method. However, the recent preparation of ditipylketene **3**[22] enabled a more general synthesis of **2a**−**2c**. The α-H enol **2a** was prepared by $LiAlH_4$ reduction of **3** and reaction with MeLi or *t*-BuLi gave, respectively, **2b** and **2c** (eq 1), which were identified by conventional methods.

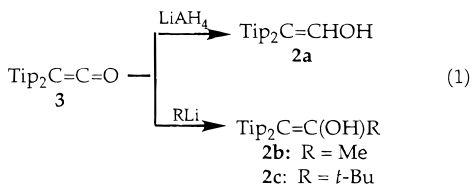

(1)

Solid-State Structure of 2,2-Ditipylethenol (2a). Enol **2a** crystallized from AcOH in the $P2_1/c$ space group as tetramers of four crystallographically independent molecules held by hydrogen bonds between the hydroxyl groups (Figure 1). The ORTEP drawing and the stereoview of one of the structures of **2a** are shown in Figure 2. Table 1 summarizes selected structural data for the four symmetry-independent structures of **2a** and comparative data for 2,2-dimesitylethenol (**1a**).[23] The four structures in the unit cell differ only slightly in their bond lengths and angles (Table 1). The enol exists in a chiral propeller conformation in which all the rings are twisted in the same direction. The solid-state structures of **1a** and **2a** are partially similar, despite the increased bulk of the isopropyl groups compared with methyl. This is mainly due to the fact that the four *o*-isopropyl groups are arranged so that the methine C−H bonds and the rings are nearly coplanar and the methine hydrogens point toward C_β. However, the *i*-Pr-methyls of **2a** radiate from the ring plane and could sterically interact (in contrast with **1a**) with a neighboring ring.

The average bond lengths of the four symmetry-independent molecules of **2a** are close to those of **1a** whereas the average bond angles somewhat differ: α_1, α_2, and α_6 are smaller but α_3 is larger by ≤2.5° in **2a** than in **1a**. In the aryl torsional angles of **2a** ϕ_1 is 2.3° smaller than in **1a** but ϕ_2 is larger by 8.3°, whereas in

(22) Frey, J.; Rappoport, Z. *J. Am. Chem. Soc.* **1996**, *118*, 5169.

(23) Biali, S. E.; Gozin, M.; Rappoport, Z. *J. Phys. Org. Chem.* **1989**, *2*, 271.

Table 1. Selected Bond Lengths and Bond (α) and Torsion (ϕ) Angles for Enols 2a and 1a

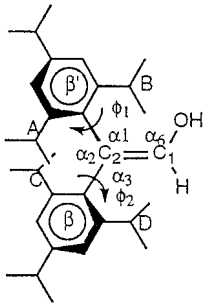

	2a[a]					
structure	1	2	3	4	average	**1a**[b]
bond lengths (Å)						
C═C	1.32(1)	1.32(1)	1.32(1)	1.34(1)	1.325	1.326
C−O	1.383(7)	1.380(9)	1.385(8)	1.357(8)	1.376	1.372
═C−Ar(β)	1.515(9)	1.53(1)	1.492(9)	1.50(1)	1.509	1.502
═C−Ar(β')	1.50(1)	1.509(8)	1.524(8)	1.49(1)	1.506	1.504
bond angles (deg)						
α_1	115.8(6)	116.9(6)	116.4(7)	117.1(5)	116.6	118.1
α_2	121.4(6)	119.6(6)	120.4(6)	121.1(6)	120.6	121.0
α_3	122.8(7)	123.4(5)	123.2(7)	121.8(5)	122.8	120.8
α_6	122.5(6)	121.4(6)	122.4(7)	123.4(5)	122.4	123.7
torsion angles (deg)						
ϕ_1	55.72	54.52	53.17	54.24	54.41	56.7
ϕ_2	58.67	59.20	58.57	59.03	58.87	50.2
nonbonded distances (Å)						
i-Pr-C(A)−C_β	2.964	2.984	2.981	2.993	2.981	3.029[c]
i-Pr-C(B)−C_β	3.071	3.075	3.065	3.080	3.232	3.002[c]
i-Pr-C(C)−C_β	2.956	2.981	2.965	2.983	2.971	2.991[c]
i-Pr-C(D)−C_β	3.065	3.044	3.044	3.073	3.056	2.971[c]
i-Pr-C(A)═CH	4.670	4.685	4.677	4.690	4.680	
i-Pr-C(B)═CH	3.989	4.027	4.026	4.020	4.016	
i-Pr-C(C)═CH	4.172	4.246	4.242	4.257	4.229	
i-Pr-C(D)═CH	2.952	2.913	2.890	2.920	2.919	
i-Pr-C(A)═C−OH	5.602	5.411	5.584	5.560	5.539	
i-Pr-C(B)═C−OH	3.401	3.648	3.499	3.561	3.526	
i-Pr-C(C)═C−OH	5.576	5.522	5.637	5.628	5.591	
i-Pr-C(D)═C−OH	4.827	4.396	4.673	4.626	4.631	
i-Pr-C(A)−*i*-Pr-C(C)	4.572	4.560	4.513	4.590	4.559	
i-Pr-C(A)−*i*-Pr-C(D)	3.525	3.543	3.747	3.734	3.637	3.766[c]
i-Pr-C(B)−*i*-Pr-C(C)	3.698	3.693	3.533	3.568	3.623	3.640[c]
i-Pr-C(B)−*i*-Pr-C(D)	6.074	6.065	6.043	6.087	6.067	

[a] 1, 2, 3 and 4 stand for the four symmetry-independent crystallographic conformations. [b] Average value of four crystallographically independent molecules, ref 4. [c] The labeling of the methyl groups (ref 4) parallels the labeling of the isopropyl methines in **2a**.

1a $\phi_1 > \phi_2$; i.e., the ring cis to the OH is more twisted relative to the double-bond plane than the ring trans to the OH, in **2a** $\phi_2 > \phi_1$. The average difference between ϕ_1 and ϕ_2 is 6.5° in **1a** and only about 4.5° in **2a** in the opposite direction.

The influence of the bulk of the α-alkyl substituent R in **1a**−**e** on the Ar−C═C torsional angle is known, but less is known on the influence of the relative bulk of the β-rings on the torsional angles. These angles reflect a compromise between their tendency to decrease in order to increase the Ar−C═C conjugation energy and to increase in order to reduce repulsive steric interactions between substituents on neighboring rings. The differences in the torsional angles of **2a** and **1a** may be due to the interaction of the *o*-*i*-Pr methyls with the geminal tipyl ring. A comparison of the solid-state structures of the 2,2-ditipylethenols **2a**−**c** could evaluate the influence of the bulk of the α-R and β-Ar ring on the ground-state conformation of **2a**−**c**, but we could not obtain single crystals of **2b** and **2c**.

Three types of relevant nonbonded distances found in **2a** are displayed in Table 1: (i) between the methine carbons and C_β, (ii) between methine carbons and vinylic H and enolic OH, and (iii) between the *o*-methines located on the same side of the double bond. These values reflect the steric crowding of the molecule and assist in the assignment of the ^{1}H NMR spectrum at low temperatures. Interestingly, both the *o*-*i*-Pr methine···C_β and β *o*-*i*-Pr methine···β' *o*-*i*-Pr methine distances are almost similar to those of the *o*-Me···C_β and β *o*-Me···β' *o*-Me found in **1a**, thus corroborating the similarity of the ground-state structures of **2a** and **1a**.

Both **2a** and **1a**[4] crystallize as hydrogen-bonded tetramers of symmetry-independent conformations. (*Z*)-2-Mesityl-2-phenylethenol[14] and 2,2-bis(pentamethylphenyl)-ethenol[10] also form solid cyclic hydrogen-bonded tetramers: in the former it is composed of two symmetry-independent conformers, and in the latter all four molecules are identical. In all these cases the C═COH conformation is *anti*. The tetrameric arrangement is unique for the α-H-β,β'-diarylethenols since it does not appear in the α-R derivatives, probably for steric reasons.

Solution Conformation of 2a. ^{1}H and ^{13}C NMR Spectra at Slow Exchange. ^{1}H NMR. The 400 MHz

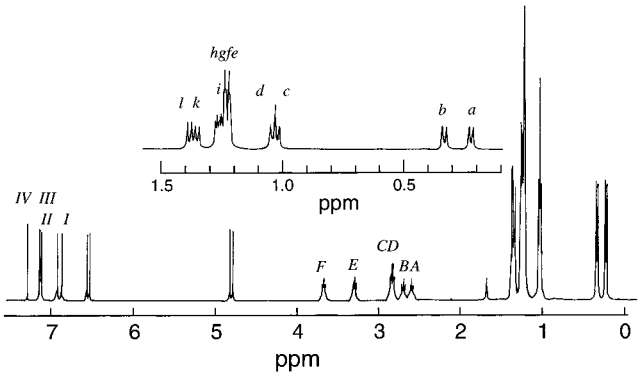

Figure 3. ^{1}H NMR spectrum of **2a** in $CDCl_3$ at 245 K. Labeling: lower case letters: isopropyl-Me's; upper case letters: isopropyl-CH; Roman numerals: Ar−H signals.

^{1}H NMR spectrum of **2a** in $CDCl_3$ at 245 K (Figure 3 and Table 2) displays distinct signals for almost all protons and isopropyl groups: nine *i*-Pr-methyl doublets (8 × 3H and 1 × 12H), five *i*-Pr-methine heptets (4 × 1H and 1 × 2H), one OH and one vinylic CH doublet (J_{HCOH} = 13.7 Hz), and four distinct aromatic doublets (J_{meta} = 1.8 Hz). Because of the prochiral character of the isopropyl group, the appearance of eight separate *i*-Pr-methyl doublets strongly suggests that in solution at 245 K **2a** adopts a chiral conformation with restricted rotations around the $C_{Ar}-C_{sp^2}$ bonds in which the *o*-isopropyls and the aromatic *m*-protons are diastereotopic. This conformation is in accord with the X-ray solid-state structure of **2a**.

We draw the three-dimensional propeller in the previously described two-dimensional projections.[8] The molecule is viewed from the π(C=C) bond plane along an axis that dissects this bond in a way that the OH is always oriented at the top right. The edge pointing to the observer is thickened and substituents on it that are above and below the molecular $C_\alpha C_\beta OH$ plane are designated as "up" and "down", respectively.

For conformational analysis and DNMR study of **2a** in solution, all the ^{1}H NMR signals should be unequivocally assigned. This requires us to distinguish the β (trans to OH) from the β' (cis to OH) tipyl rings, to identify the isopropyl moieties and their location on the tipyl rings, and to determine which aromatic proton and isopropyl groups are vicinal. A combination of COSY and NOESY experiments enabled a full ^{1}H NMR characterization of **2a** in solution at slow exchange.

The assignment of the isopropyl signals was obtained from the COSY spectrum of **2a** in $CDCl_3$ at 245 K. Figure 4 shows the aliphatic region of the spectrum in which the methyl doublets are pairwise correlated to a methine heptet, thus identifying pairs of methyl signals corresponding to the same isopropyl group. Hence, methyl doublets *a* and *d*, *b* and *c*, *i* and *l*, and *j* and *k* (for labeling, see Figure 3) are coupled to methine heptets *B*, *A*, *E*, and *F*, respectively. The larger doublet *efgh* displays a cross peak with the double-intensity heptet *CD* and was intuitively assigned to two accidentally isochronous *p*-isopropyls. This was corroborated by a NOESY spectrum (vide infra). The J_{meta} couplings of the aromatic protons observed in the 1D spectrum correlate pairwise protons *I* and *III* and *II* and *IV* (not shown). Since no ^4J crosspeaks were detected between the aromatic protons *I*−*IV* and the *i*-Pr-methines *A*−*F* we could not determine, on the basis of the COSY spectrum alone, which isopropyl is located next to which aromatic proton.

The NOESY spectrum of **2a** at 245 K in $CDCl_3$ (Figure 5) enabled a full signal assignment of the two tipyl groups. First, NOESY cross peaks were found between heptet *CD* and all of the four aromatic protons *I*−*IV*, reinforcing the assignment of the signals *CD* and *efgh* to the *p*-isopropyl groups. Second, NOESY cross peaks were found between methyl doublets *a*, *d*, and *efgh* and aromatic proton *I*, between methyls *b*, *c*, and *efgh* and proton *II*, between methyl *k* and proton *III* and between methyl *l* and proton *IV*. The correlations between methyls *efgh*, *i*, and *j* and protons *III* and *IV* could not be resolved due to the very small differences in δ's in both sets of signals. Nevertheless, since the methyl doublet pairs *i*/*l* and *j*/*k* are known from the COSY spectrum to belong each to a given isopropyl, we assume that the unresolved NOESY cross peak includes correlations for methyls *i* and *j* (as well as for methyls *efgh*) and aromatic protons *IV* and *III*, respectively. Consequently, we conclude that *A*-*bc*, *B*-*ad*, *E*-*il*, and *F*-*jk* are the *o*-isopropyls and that isopropyls *A*-*bc* and *E*-*il* together with tipyl-H *II* and *IV* belong to one ring, whereas isopropyls *B*-*ad* and *F*-*jk* and tipyl-H *I* and *III* are located on the other ring. Since the *p*-isopropyls are not resolved, *CD*-*efgh* is assigned to both rings.

The cis or trans location of each ring relative to the OH was also obtained from the NOESY spectrum (Figure 5b). Clear cross peaks were observed between the methine heptet *E* and the OH doublet and between the methine heptet *F* and the vinylic doublet. Examination of the nonbonded distances in the X-ray structure of **2a** indicates that the shortest distance between an isopropyl methine carbon and the OH group is found for the "down" *o*-isopropyl on the tipyl ring cis to the OH (*i*-Pr−C(B) in Table 1) and therefore the signals *E*-*il* are assigned to the β'-Tip ring. The shortest *i*-Pr-methine-vinylic-H distance was found for the "up" *o*-isopropyl group on the tipyl ring trans to the OH group (*i*-Pr-C(D) in Table 1), and consequently, the signals *F*-*jk* were assigned to the β-Tip ring. The full peak assignment is summarized in Figure 6.

Additional evidence for the proposed structure follows: (i) Two NOESY cross peaks in **2a** were found to correlate methines *A* and *F* and *B* and *E*. The nonbonded X-ray distances between *i*-Pr methines on different rings are the shortest between the pair of isopropyls located on the same size of the C=C plane (Table 1). Hence, the pairs of signals *A* and *F* and *B* and *E* are assigned to isopropyls located on the same side of the C=C plane. (ii) Four of the *o*-*i*-Pr methyl doublets (*a*−*d*) are shifted upfield and four (*i*−*l*) resonate downfield relative to the *p*-*i*-Pr signal. The latter signal has a δ (1.22 ppm) close to that of the methyls of 1,3,5-*i*-$Pr_3C_6H_3$ itself (1.28 ppm), which is not surprising since the *p*-substituents are the furthest from the enol moiety and will sense less the electronic and anisotropic influences of the double bond and of the neighboring tipyl ring.

Similar upfield and downfield shifts were observed for the *o*- relative to the *p*-*i*-Pr methines. Inspection of the X-ray structure and of space-filling models of **2a** confirm that in the frozen propeller conformation an "up" *o*-*i*-Pr on the β' ring and a "down" *o*-*i*-Pr on the β ring reside in the shielding region of the adjacent tipyl rings. They were therefore assigned to *A*-*bc* and *B*-*ad*, respectively. The two remaining *o*-*i*-Pr reside in the deshielding region of the neighboring tipyl rings and consequently resonate at a lower field relative to the *p*-isopropyls. Using the same reasoning, *within a given i-Pr group*, the more

Table 2. ^{1}H NMR Chemical Shifts and Peak Assignment of 2a in Several Solvents[a]

		solvent								
assignment	*b*	$CDCl_3$[c]	CD_2Cl_2[d]	$C_2D_2Cl_4$[c]	DMSO-d_6[e]	DMF-d_7[f]	THF-d_8[f]	$(CD_3)_2CO$[f]	CD_3CN[f]	$CD_3C_6D_5$[d]
β-o-i-Pr(Me)	(*a*)	0.21	0.19	0.10	0.20	0.28	0.26	0.28	0.29	0.52
	(*d*)	1.04	0.96[h]	0.93[h]	0.96	1.01[h]	1.01[g]	1.01[h]	0.99[h]	1.20[h]
β-o-i-Pr(CH)	(*B*)	2.72	2.75	2.58	2.79[i]	2.86[i]	2.88	2.93	2.83[i]	3.05
β-o-i-Pr(Me)	(*j*)	1.25	1.20	1.14[h]	1.23	1.31[h]	1.29	1.30[h]	1.22	1.33
	(*k*)	1.34	1.27	1.22	1.27	1.31[h]	1.30	1.30[h]	1.32[g]	1.36
β-o-i-Pr(CH)	(*F*)	3.70	3.69	3.58	3.65	3.77	3.77	3.78	3.68	3.82
p-i-Pr(Me)	(*efgh*)	1.22[m]	1.14	1.11	1.16[m]	1.21[m]	1.19[m]	1.19[m]	1.20[m]	1.24[g,m]
p-i-Pr(CH)	(*CD*)	2.85	2.84	2.75	2.79[i]	2.86[i]	2.80	2.85	2.83[i]	2.79
β′-o-i-Pr(Me)	(*b*)	0.33	0.29	0.20	0.27	0.36	0.37	0.38	0.37	0.60
	(*c*)	1.02	0.96[h]	0.93[h]	0.95	1.01[h]	0.99[g]	1.01[h]	0.99[h]	1.20[h]
β′-o-i-Pr(CH)	(*A*)	2.62	2.64	2.49	2.65	2.75[l]	2.74	2.76	2.68	2.95
β′-o-i-Pr(Me)	(*i*)	1.24	1.19	1.14[h]	1.19	1.28	1.26	1.28	1.27	1.25
	(*l*)	1.37	1.30	1.25	1.32	1.40	1.37	1.40	1.30[g]	1.41
β′-o-i-Pr(CH)	(*E*)	3.32	3.32	3.18	3.30[j]	3.41	3.40	3.41	3.30	3.55
=CH[n]		6.54	6.45	6.39	6.59	6.76	6.61	6.73	6.42	6.55
β-Tip-H	(*I*)	6.86	6.78	6.70	6.78[k]	6.90[g]	6.82	6.88[k]	6.87[k]	7.00
β-Tip-H	(*III*)	7.11	7.03	6.94	7.05	7.16	7.07[g]	7.13	7.12	7.19
β′-Tip-H	(*II*)	6.91	6.86	6.77	6.78[k]	6.90[g]	6.83	6.88[k]	6.87[k]	7.06
β′-Tip-H	(*IV*)	7.12	7.07	6.98	7.01	7.14	7.07[g]	7.11	7.10	7.22
OH[n]		4.83	4.75	4.74	8.92	9.32	7.76	7.97	6.59	4.44

[a] All values in δ (ppm) relative to internal TMS standard. [b] The labels refer to Figure 3. [c] At 240 K. [d] At 250 K. [e] At 298 K. [f] At 273 K. [g] dd. [h] One 2 Me doublet. [i] One 3H septet. [j] Approximate value since the signal overlaps the water signal. [k] One 2H singlet. [l] Overlaps the DMF septet. [m] Integrates for 12H. [n] For the coupling constants, see Table 4.

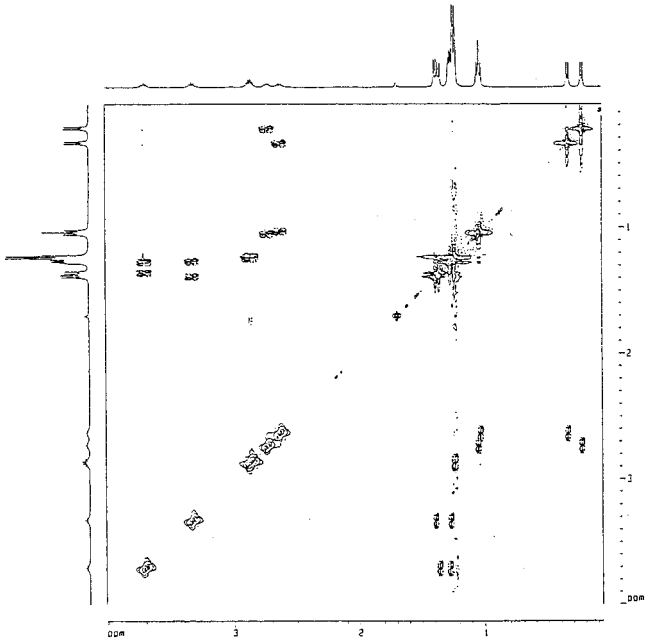

Figure 4. COSY spectrum of the aliphatic and vinylic region of **2a** in $CDCl_3$ at 245 K.

shielded doublet is assigned to the Me pointing toward the neighboring ring, as deduced from the X-ray structure and space-filling models. Within the distinct isopropyl groups, the $\Delta\delta$ (ppm) values between the two diastereotopic Me doublets are significantly larger for the *i*-Pr possesing a shielded Me group ($\Delta\delta$ (ppm) *A-bc* = 0.69; *B-ad* = 0.83) than for the deshielded ones ($\Delta\delta$ (ppm) *E-il* = 0.13; *F-jk* = 0.09).

The nonequivalence of all *o-i*-Pr methyls provides information related to the orientation of the different *i*-Pr groups in the molecule. Spectroscopic and computational studies on C_6H_5Pr-*i* have shown that out of the three possible conformations of the *i*-Pr group relative to the ring the planar conformation (Chart 1), in which the *i*-Pr-methine hydrogen eclipses the ring plane, is the most stable.[24,25a] The rotational barrier about the $C_{sp^2}-C_{sp^3}$ bond in C_6H_5Pr-*i* is 0.25 kcal mol^{-1} (low resolution MW),[25b] 2.0 kcal mol^{-1} (NMR),[25c] and 2.3 kcal mol^{-1} (calculations).[25d] Because of the low barrier, NMR studies have been unable to observe and identify specific *i*-Pr conformations. The preferred orientation of the tipyl-

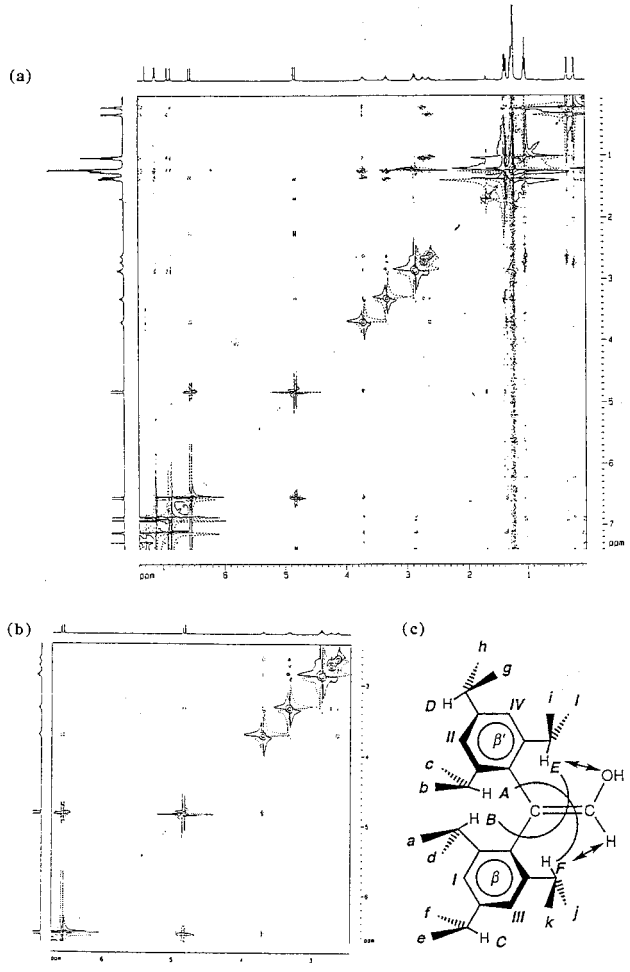

Figure 5. (a) NOESY spectrum of **2a** at 245 K in $CDCl_3$. (b) Expansion of the methine and vinyl CH and OH regions. (c) Indication of the important NOE interactions.

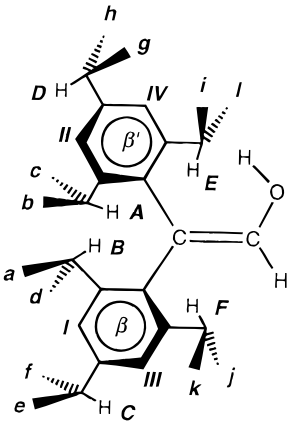

Figure 6. *Syn*-periplanar propeller conformation and full peak assignment of **2a**. The labels correspond to those in Figure 3 and in Table 2.

Chart 1

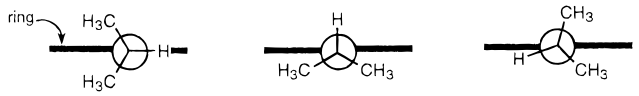

isopropyl groups of **2a** in solution was deduced from the COSY and NOESY spectra, and it considers the nonequivalence of the *i*-Pr methyls on the NMR time scale. The COSY spectrum of **2a** displayed no cross-peaks between the methine and the aromatic protons, although pairs of *m*-H were found to be mutually coupled (J_{meta} = 1.8 Hz). Since long-range H−Me couplings ($^4J_{HMe} \sim 0.75$ Hz[26a]) were reported for **1g**,[8] the lack of observed coupling between the methine and aromatic protons in **2a** suggests that the *i*-Pr groups assume a conformation in which ^4J is zero. ^4J values in allylic systems strongly depend on the torsional angle ϕ[26b] (cf. **4**). They are large for $\phi \approx 0$ or 180° and small for $\phi \approx 90$ or 270°.

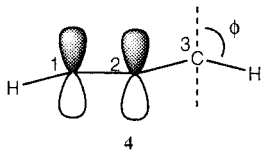

4

Introduction of large alkyl residues on C-3 leads to a preferred conformation with $\phi \approx 270°$, i.e., in which the methine C−H bond and the tipyl ring plane are nearly coplanar. This is consistent with the orientation of the *o*-isopropyls in the solid (Figure 1). The two alternative planar orientations of the *i*-Pr groups that should be considered are with the methine C−H pointing toward or away from the enolic moiety. Two NOESY cross peaks correlating the *p*-CH multiplet and two pairs of Ar−H suggest the presence of two coplanar conformations. No such correlation was found between the *o*-CH protons and their neighboring *m*-H's, thus indicating that the former

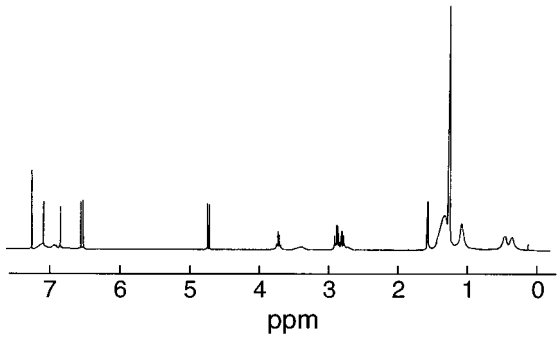

Figure 7. 400 MHz ^{1}H NMR spectrum of **2a** at room temperature in $CDCl_3$.

point toward the enol moiety, in an opposite direction to the aromatic protons. The NOESY correlations found between the Me doublets and the *m*-H's (vide supra) reinforce this suggestion.

Concerning the conformation of the *i*-Pr groups in relation to the rotation around the C_{sp^2}(Ar)-C_{sp^3}(CH) bond relative to the NMR time scale Oki emphasized that "*...NMR data do not always correspond to a single structure but sometimes correspond to an average structure*".[27] Since the average structure might be that of two or more unequally populated conformations with a larger contribution of the conformation found in the solid, we conclude that the *predominant* solution conformation of **2a** is identical with that found in the crystal.

Additional support to the proposed assignment comes from the rt spectrum of **2a** in $CDCl_3$ (Figure 7), which displays broad signals for heptets *A* and *E*, aromatic protons *II* and *IV*, and all but two methyl doublets. This broadening results from an enantiomerization process in which only one ring undergoes site exchange of the aromatic and methyl protons (vide infra). Hence, *o*-isopropyls *A-bc*, *E-il* and *m*-H's *II* and *IV* belong to one ring and *o*-isopropyls *B-ad*, *F-jk* and *m*-H's *I* and *III* belong to the other one. The appearance of the 12H *p*-isopropyl methyl doublet as two 6H doublets (*C-ef* and *D-gh*) at rt results from a temperature-dependent chemical upfield shift of one of them.

A full peak assignment of **2a** at slow exchange was achieved in $CDCl_3$ where the best resolution was achieved. The NMR spectra of **2a** were recorded in nine solvents (Table 2), and signals were assigned by analogy to the spectrum in $CDCl_3$. In poor hydrogen-bond-accepting solvents ($CDCl_3$, CD_2Cl_2, $C_2D_2Cl_4$, $C_6D_5CD_3$) the rt spectrum is broad, and a sharp and well-resolved spectrum was obtained only at ca. 250 K. In contrast, in good hydrogen-bond accepting solvents (DMSO-d_6, DMF-d_7) the rt spectrum is sharp and in solvents with moderate hydrogen-bond accepting ability (CD_3CN, $(CD_3)_2CO$, THF-d_8) the spectrum is sharp at 273 K (vide infra).

Two points deserve attention. First, δ(OH) (and J_{HCOH}, cf. Table 4) is strongly solvent dependent, as was observed for di- and trimesitylethenols.[12] Second, the assignment of the Tip-H protons in the good hydrogen-bond-accepting solvents differs somewhat from that in the weak hydrogen-bond acceptors. The aromatic protons were labeled (*I*−*IV* in Figure 3) following their $\delta(CDCl_3)$ from high to low field and were then assigned pairwise to the β-Tip (*I* and *III*) and to the β'-Tip (*II* and *IV*). In good hydrogen-bond-accepting solvents the assignment

(24) Eliel, E. L.; Willen, S. H. *Stereochemistry of Organic Compounds*; Wiley: New York, 1994; p 626.

(25) (a) Seeman, J. I.; Secor, H. V.; Breen, P. J.; Grassian, V. H.; Bernstein, E. R. *J. Am. Chem. Soc.* **1989**, *111*, 3140. (b) True, N. S.; Farag, M. S.; Bohn, R. K.; MacGregor, M. A.; Radakrishnana, J. *J. Phys. Chem.* **1983**, *87*, 7, 4622. (c) Schaefer, T.; Parr, W. J. E; Danchura, W. *J. Magn. Reson.* **1977**, *25*, 167. (d) Kao, J. *J. Am. Chem. Soc.* **1987**, *109*, 3817.

(26) Günther, H. *NMR Spectroscopy*; Wiley: Chichester, 1980; (a) pp 384−385; (b) pp 117−8.

(27) Oki, M. *Applications of Dynamic NMR Spectroscopy to Organic Chemistry*; VCH: Deerfield Beach, FL, 1985; p 199.

Table 3. ^{13}C NMR Chemical Shifts and Assignment of 2a in Two Solvents

	solvent			solvent	
assignment	$CDCl_3$[a]	DMSO-d_6[b]	assignment	$CDCl_3$[a]	DMSO-d_6[b]
i-Pr-Me	22.60	22.39	*p*-*i*-Pr-CH	33.84	33.14
	22.75	22.48		33.94	33.21
	23.89	23.75	C_β	110.48	108.47
	23.93[c]	23.81	*m*-Tip-C	121.28	120.20
	24.05	23.88[c]		122.15	120.64
	24.07	23.91		122.43	121.27
	24.13	24.00		122.75	121.66
	24.54	24.11	*ipso*-Tip-C	129.69	133.51
	24.64	24.53		134.05	135.84
	26.29	25.70	C_α	143.69	144.65
	27.21	26.83	*o*,*p*-Tip-C	146.85	145.69
o-*i*-Pr-CH	29.79	29.06		147.28	145.98
	29.89	29.18		147.54	146.79
	30.16[c]	29.75		148.03	147.07
		30.22		148.33	147.38
				149.46	147.69

[a] At 245 K. [b] At 298 K. [c] Double intensity.

Table 4. Coalescence Data for Tip_2C=CHOH (2a) at 400 MHz

solvent	process	$\Delta\nu$, Hz	T_c, K	$\Delta G_c^{\ddagger}$, kcal mol^{-1}
DMSO-d_6	β′-*o*-*i*-Pr-Me ⇌ β′-*o*-*i*-Pr-Me	15.2[c]	319.4	16.5
	β′-*o*-*i*-Pr-Me ⇌ β′-*o*-*i*-Pr-Me	303.6[d]	362[e]	16.6
	β′-*o*-*i*-Pr-CH ⇌ β′-*o*-*i*-Pr-CH	263.0[a]	345.3[a]	15.9[a]
	β′-*m*-Tip-H ⇌ β′-*m*-Tip-H	89.9	341.5	16.5
	β-*o*-*i*-Pr-Me ⇌ β-*o*-*i*-Pr-Me	369.3[f]	360[e]	16.4
	β-*o*-*i*-Pr-Me ⇌ β-*o*-*i*-Pr-Me	146.2[g]	350[e]	16.6
	β-*o*-*i*-CH ⇌ β-*o*-*i*-Pr-CH	341.9	403.6	18.5
	β-*m*-Tip-H ⇌ β-*m*-Tip-H	108.3	381.5	18.3
$C_2D_2Cl_4$	β′-*o*-*i*-Pr-Me ⇌ β′-*o*-*i*-Pr-Me	28.0[b,c]	300.6	15.1
	β′-*o*-*i*-Pr-Me ⇌ β′-*o*-*i*-Pr-Me	308.1[b,d]	325[e]	14.8
	β′-*o*-*i*-Pr-CH ⇌ β′-*o*-*i*-Pr-CH	280.9[b]	322.0	14.8
	β′-*m*-Tip-H ⇌ β′-*m*-Tip-H	82.4[b]	312.7	15.1
	β-*o*-*i*-Pr-Me ⇌ β-*o*-*i*-Pr-Me	360.1[b,f]	325[e]	14.7
	β-*o*-*i*-Pr-Me ⇌ β-*o*-*i*-Pr-Me	136.0[b,g]	325[e]	14.8
	β-*o*-*i*-Pr-CH ⇌ β-*o*-*i*-Pr-CH	392.7[a]	405.6	18.4
	β-*m*-Tip-H ⇌ β-*m*-Tip-H	98.0[a]	381.2	18.4
$C_6D_5CD_3$	β′-*o*-*i*-Pr-Me ⇌ β′-*o*-*i*-Pr-Me	13.4[c]	291.0	15.0
	β′-*o*-*i*-Pr-Me ⇌ β′-*o*-*i*-Pr-Me	273.3[d]	322[e]	14.8
	β′-*o*-*i*-Pr-CH ⇌ β′-*o*-*i*-Pr-CH	237.2	320.0	14.8
	β′-*m*-Tip-H ⇌ β′-*m*-Tip-H	64.0	305.6	14.9

[a] See text. [b] Measured in CD_2Cl_2 (see text). [c] *i*-Pr-Me's "j" and "k" in Table 2. [d] *i*-Pr-Me's "a" and "d" in Table 2. [e] ±5 K, see text. [f] *i*-Pr-Me's "b" and "i" in Table 2. [g] *i*-Pr-Me's "c" and "l" in Table 2.

differs from the labeling used in $CDCl_3$ as shown by comparing the rt spectra of **2a** in the various solvents. Whereas in $CDCl_3$ and other weak hydrogen-bond acceptors the second and fourth protons (*II* and *IV* in Figure 6) are broadened, in the good hydrogen-bond-accepting solvents the second and third Ar−H are broad. (Although in DMSO-d_6, DMF-d_7, CD_3CN, and $(CD_3)_2CO$ the two most upfield Tip-H protons are accidentally isochronous, in THF-d_8 they are resolved and the second proton is broad; we assume analogy of the spectrum in THF-d_8 to that in the other solvents). Since the ring undergoing site exchange at rt is β′, the assignment was determined accordingly (vide infra).

^{13}C NMR. The 100 MHz ^{13}C NMR spectrum of **2a** in $CDCl_3$ at 245 K displayed distinct signals for all but two of its 32 carbons (Table 3). One Me- and one CH signal showed double intensity due to accidental isochrony. At rt most signals were broad. A similar spectrum in DMSO-d_6 at rt shows only one accidentally isochronous Me signal. The peak assignment was by gated decoupled ^{13}C NMR spectra. However, we could not distinguish the *o*- from the *p*-isopropyl methyls or the various Tip-C's. A frozen conformation on the NMR time scale is again indicated.

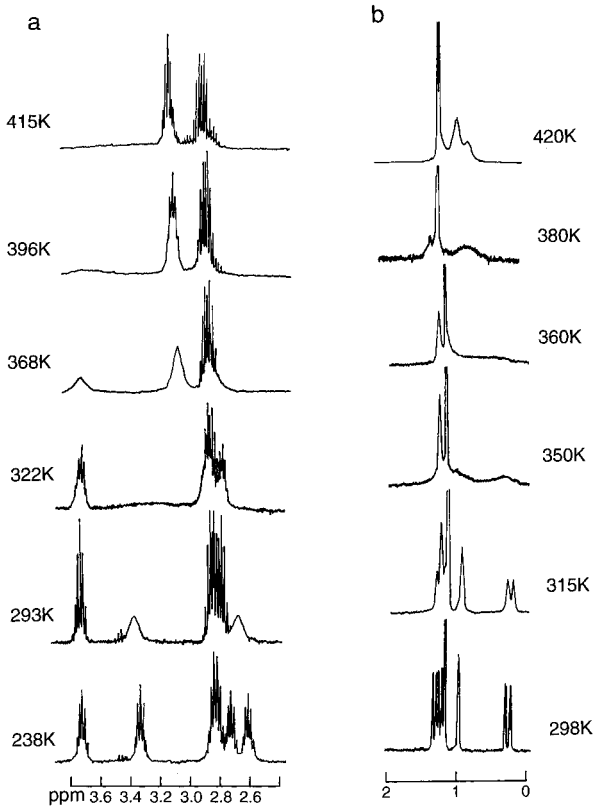

Figure 8. ^{1}H NMR spectra of the (a) *i*-Pr-methine and (b) *i*-Pr-methyl regions of **2a** in DMSO-d_6 (a) and CD_2Cl_2 and $C_2D_2Cl_4$ (b) at various temperatures.

A comparison of $\delta(C_\alpha)$ and $\delta(C_\beta)$ for **2a** and **1a** ($\delta(C_\beta) = 112.77$, $\delta(C_\alpha) = 143.89$ in $CDCl_3$ at 75 MHz at 223 K)[9b] shows that the change Mes → Tip is somewhat stronger on C_β than on C_α. This might reflect the higher steric congestion at C_β since at C_α both molecules are rather similar.

In contrast to the ^{1}H NMR spectrum (Table 2) the ^{13}C spectrum (Table 3) is only slightly affected by the solvent's hydrogen-bond-accepting ability. Mostly affected are C_α and C_β. In DMSO-d_6 C_β is shifted upfield by 2 ppm and C_α is shifted downfield by 1 ppm relative to $CDCl_3$. This is consistent with computations showing an upfield shift of C_β and a downfield shift of C_α on association with a hydrogen-bond-accepting solvent.[28] It was shown computationally that hydrogen bonding polarizes the O−H bond in the sense $O^{\delta-}\cdots H^{\delta+}$. Hence, the more negatively charged oxygen (in **2a**·DMSO vs **2a**) will delocalize the charge better to C_β with its consequent shift to a higher field and of C_α to a lower field.

Dynamic Stereochemistry of 2a. The rt ^{1}H NMR spectra of **2a** in poor hydrogen-bond-accepting solvents displayed several broad signals for all the *i*-Pr-Me, the β′*o*-*i*-Pr−CH's and the β′-Tip-H's. On raising the temperature, additional signals broadened and several coalescence processes were observed. Figure 8 shows the temperature dependence of the ^{1}H NMR spectra of the *i*-Pr-methyl (in DMSO-d_6) and *i*-Pr-methine (in CD_2Cl_2 and $C_2D_2Cl_4$) region of **2a**, and Figure 9 displays experimental and calculated ^{1}H NMR spectra in the aromatic region in CD_2Cl_2 and $C_2D_2Cl_4$ at various temperatures (experimental) and rate constants (simulated). The coalescence data are given in Table 4.

(28) Frey, J.; Eventova, I.; Rappoport, Z.; Muller, T.; Takai, Y.; Sawada, M. *J. Chem. Soc., Perkin Trans. 2* **1995**, 621.

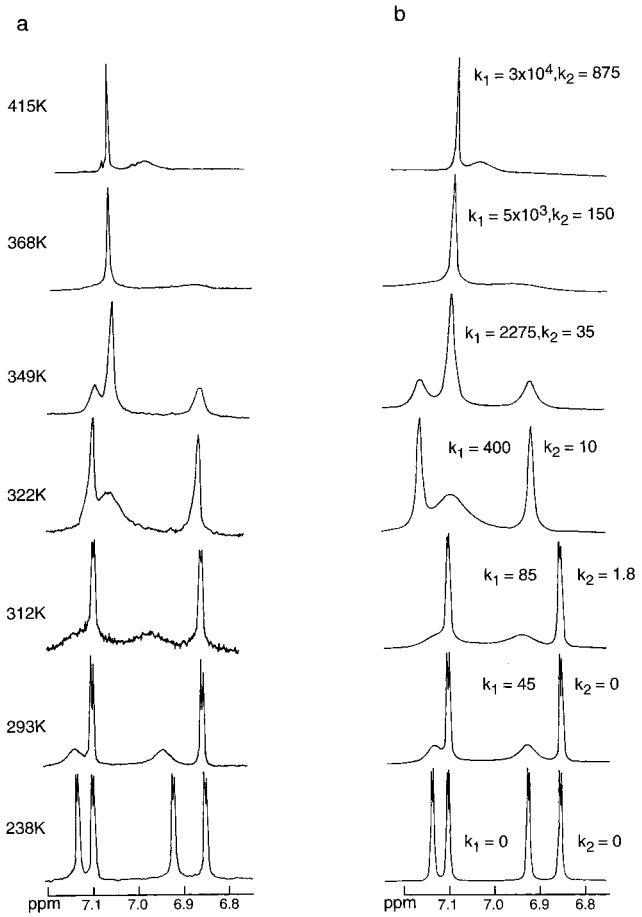

Figure 9. Experimental (a) and simulated (b) ^{1}H NMR spectra of the aromatic region of **2a** in CD_2Cl_2 and $C_2D_2Cl_4$ at various temperatures.

The dynamic processes undergone by **2a** at ca. 240 to >400 K require the use of low-melting and high-boiling solvents. In spite of its high mp, DMSO-d_6 was found suitable since a sharp and well-resolved slow exchange spectrum was obtained at rt. In $C_6D_5CD_3$ a sharp spectrum was obtained at ca. 250 K, but its boiling point precluded measurements in the fast exchange regime. In $C_2D_4Cl_2$, at 245 K, the high viscosity of the solution resulted in a broad spectrum. We therefore measured the low-temperature spectra in CD_2Cl_2 and assumed that the similarity of the two solvents permits neglect of solvent effects on the stereodynamic properties of **2a**.

The exchange rates (k_c) at the coalescence temperature (T_c) were calculated by using the Gutowsky−Holm approximation[29] ($k_c = \pi\Delta\nu/\sqrt{2}$) for the isopropyl methines and methyls and by using the equation $k_c = (\pi/\sqrt{2})(\sqrt{\Delta\nu^2 + J^6})$ for the mutually coupled *m*-tipyl protons.[30] The rotational barriers ($\Delta G_c^{\ddagger}$) were obtained from the Eyring equation assuming a transmission coefficient of unity.[31] We calculated $\Delta G_c^{\ddagger}$ from the coalescence data of *o*-*i*-Pr-Me pairs when possible, and of *o*-*i*-Pr-CH and aromatic protons pairs. The $\Delta G_c^{\ddagger}$ values obtained from either process were mostly similar. Discrepancies of 0.1−0.6 kcal mol^{-1} between the barriers calculated by the three probes are ascribed to experimental errors caused by the following: (i) accidental overlap of the water signal (present in the DMSO-d_6) with a β'-*o*-*i*-Pr-CH multiplet that hampers exact determination of $\Delta\nu$ and therefore of k_c; (ii) in $C_2D_2Cl_4$ the $\Delta\nu$ value used was the value measured in CD_2Cl_2 at 240 K, which could result in a different k_c value; (iii) the *o*-*i*-Pr-Me and *o*-*i*-Pr-CH probes should be less accurate since additional, usually broad, peaks appear between the coalescing signals making the accurate determination of T_c difficult. Because of the uncertainty of both the $\Delta\nu$ of the *i*-Pr-Me signals involved in the high energy process (see below) and their T_c value, we calculated $\Delta G_c^{\ddagger}$ for this process only from the *i*-Pr-CH and Tip-H signals. Since the dynamic processes took place at T_c > 400 K, due to instrument limitation we were not always able to detect a sharp average post-exchange peak that usually sharpens at ca. 20° > T_c.

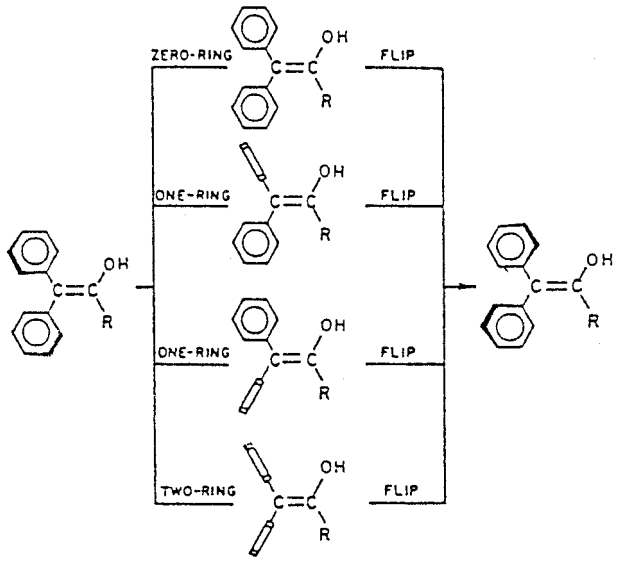

Figure 10. Idealized transition states for the flip mechanisms of a 2,2-diarylethenol propeller. The rectangular projection represents a ring that is pependicular to the C=C plane.

Three interesting points arise from Table 4. (i) Two different processes are clearly observed, each involving site exchange of *o*-*i*-Pr-CH and *m*-Tip-H signals at a different tipyl ring: a low energy process for the β'-ring and a high energy process for the β-ring. Total line shape simulations of the *m*-Tip-H coalescence processes agree with this observation (Figure 9) and yield k's from which $\Delta G_c^{\ddagger}$ values similar to those in Table 4 are obtained. (ii) Whereas only the β'-*o*-*i*-Pr-CH and *m*-Tip-H signals are involved in the low energy process, both β and β'-*i*-Pr-Me's coalesce in this process. (iii) The low energy barrier in DMSO-d_6 is 1−1.5 kcal mol^{-1} higher than those in $C_2D_2Cl_4$ and $C_6D_5CD_3$. A similar solvent effect, albeit on both the low and high energy barriers, was observed for **1a** in CD_2Cl_2/CS_2 vs $(CD_3)_2CO$ ($\Delta\Delta G_c^{\ddagger}$= 1.7 kcal mol^{-1}).[10] The high energy barrier for **2a** is solvent-independent.

Four different flip mechanisms of correlated rotation can be envisioned for 1,1-diarylvinyl propellers. Their idealized transition states are schematically depicted in Figure 10. Rotations of none, one, or two rings by 180° while the nonrotating rings remain fixed, which do not involve helicity reversal, should also be considered.

In analyzing the dynamic processes the different magnetic sites of one enantiomer of **2a** were labeled by lower case letters for *i*-Pr-methyls, by upper case letters for *i*-Pr-methines, and by Arabic numerals for the *meta*-Ar-H (Figure 11). The orientation of the diastereotopic *i*-Pr-methyls relative to the tipyl ring plane is represented

(29) Gutowski, H. S.; Holm, C. H. *J. Chem. Phys.* **1964**, *40*, 2426.
(30) Kurland, R. J.; Rubin, M. B.; Wise, W. B. *J. Chem. Phys.* **1964**, 40, 2426.
(31) Sandström, J. *Dynamic NMR Spectroscopy*; Academic Press: London, 1982; Chapter 6, p 77.

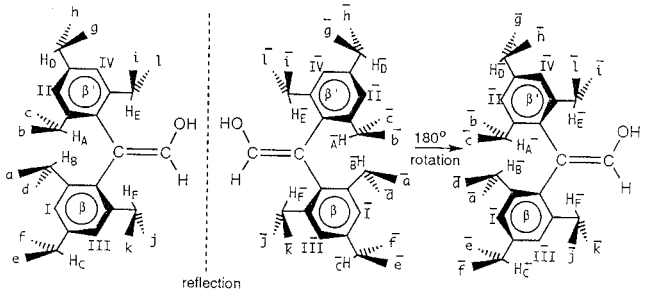

Figure 11. Relationship between the two enantiomers of **2a** and their enantiotopic sites.

by solid and dashed wedges for methyls pointing above and below the ring plane, respectively. The enantiotopic sites (by external comparison) are assigned the same letters with an overbar, i.e., methyls a and ā are enantiotopic. To facilitate the analysis, **2a** is reoriented at the right of Figure 11. The sites exchanged by the different flip and 180° rotation processes are summarized in Table 5.

An enantiomerization via a flip of a given ring will be accompanied by coalescence of three sets of NMR signals, i.e., *o*-*i*-Pr-CH, *m*-Tip-H, and *o*-*i*-Pr-Me signals. Helicity reversal via a nonflipping route involves only the coalescence of *i*-Pr-Me signals, while the Tip-H and *i*-Pr-CH remain unchanged. In the 180° rotations, all the magnetic sites of the rotating ring(s) are exchanged. The sites exchanged in the Tip-H and *i*-Pr-CH coalescences are identical with those described for the *o*-Me and *m*-Mes-H signals in **1a**, and the information derived from these processes should suffice to determine the rotational mechanisms of **2a**. However, the coalescence data for the *i*-Pr-Me signals adds valuable *direct* information that completes the unequivocal identification of the enantiomerization mechanism. The two types of diastereotopic *i*-Pr-Me site exchange involve two methyls on either one isopropyl or on different isopropyls. Whereas the former process defines the process unambiguously as an enantiomerization, the latter does not necessarily imply enantiomerization. Site exchange of two geminal *o*-Pr-methyls will occur only when, along the rotational process, the isopropyl is bisected by the molecular plane of symmetry. In contrast, the two *p*-*i*-Pr-methyls will coalesce when the tipyl ring rotation involves a conformation in which the ring is either coplanar with or perpendicular to the C=C double bond plane, assuming that rotation about the Ar-*i*-Pr bonds is faster than Ar−C=C bond rotation. Site exchange of two *o*-i-Pr-Me's located on different isopropyls will occur when during the rotation the ring passes through a plane perpendicular to the C=C bond (e.g., in a ring flip mechanism).

Three conclusions regarding the low energy process undergone by **2a** arise from the coalescence data. (i) According to the *β*′-Tip-H and *β*′-*i*-Pr-CH coalescence processes (and their absence in the *β*-Tip counterpart) and from the *β*- and *β*′-*i*-Pr-Me exchanging sites the mechanism is a [*β*′]-one-ring flip. (ii) The flip of the *β*′-Tip and the nonflip rotation of the *β*-Tip rings are correlated since the $\Delta G_c^{\ddagger}$ values for all the probes, including the *β*-*i*-Pr-Me are identical within experimental error. This conclusion requires additional computational support.[5] (iii) The [*β*′]-one-ring flip is the threshold enantiomerization mechanism of **2a** since the $\Delta G_c^{\ddagger}$ value for the averaging of the diastereotopic geminal *β*-*i*-Pr-Me's is identical with those measured for the *β*′-Tip-ring rotation. Hence, no lower energy process could be responsible for the enantiomerization.

An unequivocal identification of the high energy process undergone by **2a** is more difficult. The coalescence data for the *β*-Tip-H and *β*-*i*-Pr-CH probes are consistent with either a [*β*,*β*′]-two-ring flip or a sequential [*β*′]- and [*β*]-one-ring flip processes (Table 5). The "ideal spectrum" of the *i*-Pr-Me region at fast [*β*′]-one-ring flip should display four average peaks for the exchanging pairs: (bī,ib̄), (cl̄,lc̄), (ad̄,dā), and (kj̄,jk̄). In a [*β*,*β*′]-two-ring flip process magnetic site exchange between *o*-*i*-Pr-Me's on different *β*-ring isopropyls should yield 3 average *o*-*i*-Pr-Me signals after coalescence [(bī,ib̄), (cl̄,lc̄), (ad̄,dā), and (kj̄,jk̄)]. In contrast, in the sequential two one-ring flip processes only two average post-coalescence peaks for protons (bīcl̄,ib̄lc̄) and (ad̄kj̄,dājk̄) will appear, since the nonflip process of the *β*′-Tip ring should exchange magnetic sites on a certain *i*-Pr as well. From Figure 8a this ambiguity cannot be unequivocally resolved since at ca. 440 K two broad *o*-*i*-Pr-Me peaks (and 2 sharp *p*-*i*-Pr-Me doublets) appear and it is unclear whether one of them will split into two after sharpening at a higher unattainable (on the NMR spectrometer) temperature. A similar uncertainty concerning the higher energy process in **1a** was solved by MM calculations of the transition state energies of the various possible routes:[5] the calculated [*β*,*β*′]-two-ring flip barrier gave the best fit with experiment. Furthermore, $\Delta G_c^{\ddagger}$ for the [*β*,*β*′]-two-ring flip processes of **1a**−**e** correlate linearly with Taft's steric parameter (E_s), thus reinforcing the identification of the second process as a two-ring flip (vide infra). In our case, calculations were unsuccessful (see below) and we can only assume that the similar behavior of **2a** and **1a** for the low energy process will also hold for the high energy process.

The tipyl groups of **2a** served as intrinsic enantiomerization probes for a relatively unambiguous study of the stereodynamic processes. For **1a**, which lacks such probes, the isopropyl ether **5** was applied for further delineating the rotational mechanism, and it was concluded that the [*β*′]-one-ring flip is the threshold mechanism. A low energy nonhelicity reversal process was ruled out by the identity of the rotational barriers ($\Delta G_c^{\ddagger}$ [*o*-Me ⇌ *o*-Me]) and the enantiomerization barrier ($\Delta G_c^{\ddagger}$ [*i*-Pr-Me ⇌ *i*-Pr-Me]) of **5**.

$Mes_2C{=}CHOPr\text{-}i$
5

The relatively large solvent effect on the [*β*′]-one-ring flip barrier and its absence on the [*β*,*β*′]-two-ring flip (Table 4) are noteworthy. In poor hydrogen-bond-accepting solvents the OH of **1a** hydrogen bonds with the ring cis to it (Ar)[12] and this interaction should stabilize the *syn* periplanar C=COH conformation. The fact that in the threshold mechanism the flipping ring is the *β*′-Tip, rather than the *β*-Tip, suggests that the OH···*π*(Ar) interaction modifies the ground-state conformation of **2a** as to facilitate the flip process. Since increasing the Ar−C=C torsional angle in **1a**−**e** reduces $\Delta G_c^{\ddagger}$, we propose that the *syn*-periplanar OH increases the *β*′-Tip-C=C torsional angle of **2a** compared with the *anti*-solvent hydrogen-bonded conformation and consequently lowers the activation barrier for enantiomerization. Due to the lack of such OH···*π*(*β*-Tip) interaction the solvent change should not affect the high energy barrier. Similarly, the rotation barrier for 2-hydroxybiphenyls differed by up to

Table 5. Sites Exchanged by Flip and 180° Rotation Routes

ring flip	flipping	site	rotating	site
zero-ring	[none]	(AĀ)(EĒ)(DD̄)(BB̄)(FF̄)(CC̄) (I Ī)(III III)(II II)(IV IV) (ad̄)(dā)(kj̄)(jk)(ef̄)(fē) (bc̄)(cd̄)(il̄)(lī)(hg̃)(gh)	[none]	(AA)(EE)(DD)(BB)(FF)(CC) (I I)(III III)(II II)(IV IV) (aa)(dd)(kk)(jj)(ee)(ff) (bb)(cc)(ii)(ll)(hh)(gg)
one-ring	[β]	(BF̄)(FB̄)(CC̄)(AĀ)(EĒ)(DD̄) (I III)(III I)(II II)(IV IV) (ak̄)(kā)(dj̄)(jd̄)(eē)(ff̄) (bc̄)(cb̄)(il̄)(lī)(hg̃)(gh)	[β]	(BF)(FB)(CC)(AA)(EE)(DD) (I III)(III I)(II II)(IV IV) (aj)(ja)(dk)(kd)(ef)(fe) (bb)(cc)(ii)(ll)(hh)(gg)
one-ring	[β']	(AĒ)(EĀ)(DD̄)(BB̄)(FF̄)(CC̄) (II IV)(IV II)(I Ī)(III III) (bī)(ib)(cl̄)(lc̄)(hh)(gg̃) (ad)(dā)(kj)(jk)(ef)(fē)	[β']	(AE)(EA)(DD)(BB)(FF)(CC) (II IV)(IV II)(I I)(III III) (bc)(cb)(il)(li)(hg)(gh) (aa)(dd)(kk)(jj)(ee)(ff)
two-ring	[β,β']	(AĒ)(EĀ)(DD̄)(FB̄)(BF̄)(CC̄) (I III)(III I)(II IV)(IV II) (ak̄)(kā)(dj̄)(jd̄)(eē)(ff̄) (bī)(ib)(cl)(lc̄)(hh)(gg)	[β,β']	(AE)(EA)(DD)(BF)(FB)(CC) (I III)(III I)(II IV)(IV II) (aj)(ja)(dk)(kd)(ef)(fe) (bc)(cb)(il)(li)(hg)(gh)

[a] E.g., (ad̄) designates a site exchange between the magnetic sites "a" and "d̄" in Figure 11.

1.7 kcal mol^{-1} in different solvents according to their hydrogen-bond-accepting ability.[32]

To corroborate the conclusions regarding the enantiomerization of **2a**, we attempted to calculate some of the possible transition-state structures for the processes by molecular mechanics (MM2 as implemented in Macromodel). Unfortunately, presumably due to the high steric demands, the calculations did not converge to a chemically significant energy minimum, the tipyl rings were highly distorted, and introduction of planarity constraints of the rings precluded convergence.

The 6 and 5 kcal mol^{-1} higher rotational barriers for **2a** compared with **1a** for the one- and the two-ring flip, respectively, in halogenated hydrocarbon solvents reflect an increased steric hindrance. These large differences are remarkable in view of the generally similar ground-state structures of both enols. Akkerman[21] had demonstrated that $\Delta G^{\ddagger}$ for the racemization of bis(3-methyltipyl)-acetic acid consisted of a large entropy and a relatively low enthalpy contribution. The total line-shape analysis used to simulate the spectra of the aromatic protons of **2a** in CD_2Cl_2 and $C_2D_2Cl_4$ at various temperatures (Figure 9) yielded k's from which for the one-ring flip $\Delta H^{\ddagger} = 13.5$ kcal mol^{-1}, $\Delta S^{\ddagger} = -5.4$ eu ($R = 0.995$, SD = 0.13) and for the two-ring flip $\Delta H^{\ddagger} = 14.2$ kcal mol^{-1}, $\Delta S^{\ddagger} = -11.0$ eu ($R = 0.987$, SD = 0.14). Unfortunately, a similar simulation for **1a** did not produce an acceptable fit between experimental and calculated spectra, primarily due to extensive temperature-dependent chemical shifts and line broadening. Since **1a** reaches the slow exchange regime only at <150 K the spectra measured at 150 K are broad due to the solvent's viscosity.

The $\Delta H^{\ddagger}$ values for **2a** are very similar for both processes, and the $\Delta G^{\ddagger}$ differences result mainly from different $\Delta S^{\ddagger}$ terms. The more negative $\Delta S^{\ddagger}$ for the two-ring flip compared with the one-ring flip is consistent with Akkerman's observation[21,33] of the high $\Delta S^{\ddagger}$ for the racemization of the bis(3-methyltipyl)acetic acid by a two-ring flip process. The close $\Delta H^{\ddagger}$ values calculated for the two transition states may be fortuitous. The $\Delta H^{\ddagger}$ (**2a**) value for the two-ring flip process resembles the $\Delta G^{\ddagger}$ (**1a**) in a CS_2/CD_2Cl_2 mixture (14.2 vs 13.5 kcal mol^{-1}). This could suggest that $\Delta G^{\ddagger}$ for rotation in **1a** is mainly enthalpic, although we have no evidence for the low $\Delta S^{\ddagger}$ contribution to $\Delta G_c^{\ddagger}$ in **1a**. The mesityl, with its conical methyl substituents, may induce less entropy changes between the ground and transition states than tipyl whose isopropyls lack this symmetry.

Table 6. β(OH), δ(α-CH), and $^3J_{HCOH}$ values for Tip$_2$C=CHOH (2a) and Mes$_2$C=CHOH (1a) in Several Solvents at Room Temperature

			2a[a,b]			**1a**[a,c]		
no.	solvent	β	δ(OH)	δ(CH)	$^3J_{HCOH}$	δ(OH)	δ(CH)	$^3J_{HCOH}$
1	DMSO-d_6	0.76	8.92	6.59	5.6	9.01	6.5	5.9
2	DMF-d_7	0.69	9.08	6.75	6.2	9.17	6.6	4.6
3	THF-d_8	0.55	7.54	6.59	8.1	7.51	6.4	9.2
4	CD_3COCD_3	0.48	7.68	6.72	6.8	7.65	6.5	8.2
5	CD_3CN	0.31	6.59	6.23	7.0	6.22	6.5	8.6
6	$C_6D_5CD_3$	0.10	4.32	6.54	12.8	4.30	6.2	12.3
7	$CDCl_3$	0.00	4.72	6.52	13.5	4.66	6.4	13.5
8	CD_2Cl_2	0.00	4.77	6.50	12.8	4.72	6.4	12.9
9	CCl_4	0.00	4.42	6.35	13.8	4.47	6.3	14.1

[a] All chemical shifts are relative to internal TMS standard. [b] At 298 K. [c] At 296 K, from ref 12a,b.

Conformation of the C=COH Moiety. δ(OH) and $^3J_{HCOH}$ in Pure Solvents. The rt ^{1}H NMR spectrum of **2a** was measured in nine solvents differing in their polarity and hydrogen-bond-accepting ability. Table 6 summarizes the δ(OH), δ(α-CH), and $^3J_{HCOH}$ values for **2a** and those previously measured for **1a**[12a] and the solvents' Kamlet−Taft solvatochromic parameter β.[34] Both δ(OH) and $^3J_{HCOH}$ are strongly solvent and temperature dependent. A plot of δ(OH) [**2a**] against δ(OH) [**1a**] (Figure 12) gave a linear relationship with a slope of 1.02 ($R = 0.998$, SD = 0.13), indicating that both enols interact similarly with the solvent. A plot of the Kamlet−Taft β vs δ(OH) for **2a** was also linear ($R = 0.981$, SD = 0.35) (Figure S1, Supporting Information).

We conclude that, as for **1a**, (i) the large δ(OH) shifts on changing the solvent result from OH association with the hydrogen-bond-accepting solvents, that (ii) **2a** adopts different C=COH arrangements in different solvents according to their hydrogen-bond-accepting abilities, and that (iii) the different conformers interconvert rapidly on the NMR time scale (eq 2). In good hydrogen-bond-

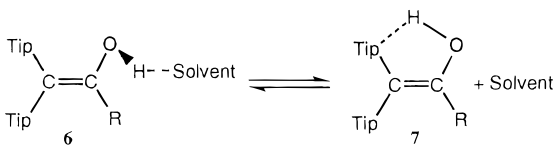

(2)

accepting solvents an *anti*-clinal conformer hydrogen

(32) See references in ref 27, p 144.
(33) Finocchiaro, P. *Gazz. Chim. Ital.* **1975**, *105*, 149.

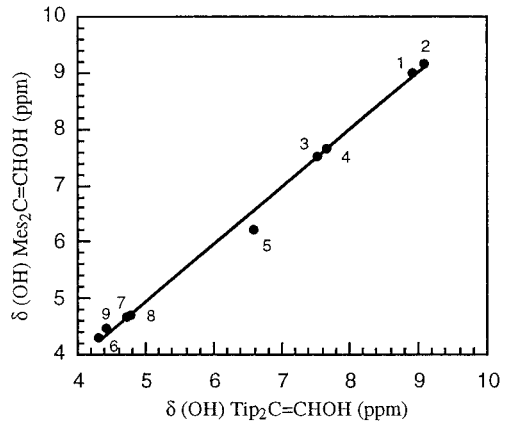

Figure 12. Plot of δ(OH) values of **1a** vs that of Tip_2C=CHOH **2a** in nine solvents at room temperature. The numbering is according to Table 6.

bonded to a solvent, **6**, predominates. In poor hydrogen-bonding solvents **2a** adopts a *syn*-(peri)planar conformation **7** that is intramolecularly OH···π hydrogen bonded to the tipyl ring cis to it.

The *syn*-planar C=CHOH conformation in non-hydrogen-bonding solvents was deduced for **1a** from the $^3J_{HCOH}$ values.[12a] A plot of $^3J_{HCOH}$(**2a**) (DMF excluded) against those of **1a** (Figure S2, Supporting Information) gave fairly linear correlation with a slope of 0.943 (R = 0.959, SD = 0.35), strengthening the suggestion of similar hydrogen-bonded conformations for both enols. However, there are also differences: (i) The $^3J_{HCOH}$ (**2a**) in both CCl_4 and DMSO-d_6 are lower than those of **1a** by 0.3 Hz. A larger difference (1.6 Hz) in the opposite direction was observed in DMF-d_7. While small $^3J_{HCOH}$ differences might result from different electronegativities of the substituents, it is more likely that they result from the slightly different conformations of **2a** and **1a** that differ in their bulk. (ii) The *syn*-planar conformation of **1a** in non-hydrogen-bond-accepting solvents is stabilized by intramolecular OH···π(*cis*-Ar) hydrogen bonding and displays a $\nu_{OH}(CCl_4)$ stretching at 3528 cm^{-1}; another stretching with 2% intensity at 3628 cm^{-1} was ascribed to a free OH, presumably in an *anti*-type conformation. In contrast, **2a** displayed only one $\nu_{OH}(CCl_4)$ at 3522 cm^{-1}, indicating a lower concentration (<1%) of the free OH conformer (if any) in CCl_4 than in **1a**. (iii) **1a** associates in solution *via* hydrogen bonding to di- or tetrameric supramolecular assemblies at low temperature, but **2a** did not show a similar association, presumably due to a stronger OH···π interaction.[35]

δ(OH) in Binary CCl_4−DMSO-d_6 Mixtures. It is possible that the geometry of the *anti*-clinal conformer (observed for **1a**)[12a] may differ in the different solvents and affect the $^3J_{HCOH}$ and δ(OH) values used for determining the conformation.[12c] The spectra of **1a**−**e** were therefore measured in binary CCl_4−DMSO-d_6 mixtures, and from the results it was concluded that only one DMSO molecule is hydrogen bonded to one enol molecule and enols/solvent association constants (K_{assoc}) were calculated.[12]

For comparing K_{assoc} values for **1a** and **2a**, we measured the ^{1}H NMR spectra of **2a** in CCl_4, in DMSO-d_6, and in their binary mixtures at 298 K. The data (Table 7) indicate a similar enol−solvent interaction for both enols. For **2a** the plots of $^3J_{HCOH}$ and δ(OH) vs [DMSO] (Figure S3, Supporting Information) are very steep at low [DMSO] and approach a plateau at [DMSO] $\approx$ 1.5 M. Addition of 0.6% (v/v) of DMSO in CCl_4 changes $^3J_{HCOH}$ from 13.8 to 9.1 Hz and δ(OH) from 4.42 to 6.66 ppm, which is ca. 50% of the overall change between CCl_4 and DMSO. As for **1a**[12a] the changes in $^3J_{HCOH}$ and δ(OH) of **2a** are linearly correlated (Figure S4, Supporting Information).

Table 7. δ(OH) and $^3J_{HCOH}$ Values and Derived Equilibrium Constants for 2a in Binary CCl_4−DMSO-d_6 Mixtures at 298 K[a]

DMSO-d_6,[b] %	[DMSO-d_6] M	$^3J_{HCOH}$, Hz	δ(OH), ppm	$F_{anti\text{-}DMSO}$[c]	K[d]	K_{assoc}
0	0	13.8	4.42	0	0	0[e]
				0	0	0[f]
0.2	0.028	12.3	5.18	0.18	0.22	10.0[e]
				0.17	0.20	8.9[f]
0.6	0.084	9.1	6.66	0.57	1.34	20.7[e]
				0.50	0.99	14.7[f]
2	0.28	7.7	7.28	0.74	2.90	11.4[e]
				0.64	1.74	6.7[f]
4	0.56	6.8	7.78	0.85	5.83	11.0[e]
				0.75	2.95	5.5[f]
10	1.4	6.1	8.22	0.94	15.4	11.2[e]
				0.84	5.43	4.0[f]
30	4.2	5.7	8.53	1.5	81.0	19.4[e]
				0.91	10.5	2.5[f]
60	8.4	5.6	8.75	1.0	∞	
				0.96	26.8	3.2[f]
80	11.2	5.6	8.83	1.0	∞	
				0.98	49.0	4.4[f]
100	14.0	5.6	8.92	1.0	∞	
				1.0	∞	

[a] [**2a**] = 0.0335 M. [b] Volume % of DMSO in a total of 10 mL solution. [c] Based on K(J). [d] Based on $K(\delta)$. [e] Calculated from eq 6a. [f] Calculated from eq 6b in the Supporting Information.

From the δ(OH) and $^3J_{HCOH}$ values in the various CCl_4−DMSO-d_6 mixtures we calculated K_{assoc} for **2a** according to eq 3 (**6a** = **6** = solvent = DMSO).

$$\mathbf{7} + \text{DMSO} \overset{K_{assoc}}{\rightleftharpoons} \mathbf{6a} \qquad (3)$$

The methods used previously[12] for calculating K_{assoc} values for **1a** assume that the associated/nonassociated enol ratio can be calculated from the δ(OH) and $^3J_{HCOH}$ values, if the solvent effect can be neglected and the two conformers interconvert rapidly on the NMR time scale. The observed δ(OH) and $^3J_{HCOH}$ values in the various CCl_4−DMSO-d_6 mixtures will then be the weighted averages of the δ and ^3J values of the pure species. The equations used for calculating K_{assoc} and the iterative procedures are similar to those published previously.[12]

The procedure is described, together with Figures S5−S7, in the Supporting Information. The K_{assoc} value for **2a**·DMSO is 6.42 L M^{-1} and the δ(OH) for the *anti*-conformation is 8.91. These values resemble K_{assoc} = 5.25 and δ(OH) (*anti*-conformation) of 9.01 for **1a**.[12]

Consequently, K_{assoc} values for **2a** and **1a** with DMSO are very similar, and from the data in pure DMSO only the *anti*-type conformer **6a**, which is associated with one DMSO molecule, is present. The 20% higher K_{assoc} for **2a** compared to **1a** is within the expected accuracy of the determination of K_{assoc} considering the known mutually dependent errors resulting from the simultaneous determination of K_{assoc} and $\delta_{anti-DMSO}$.[36]

(34) Kamlet, M. J.; Doherty, R. M.; Abraham, M. M.; Carr, P. W.; Doherty, R. F.; Taft, R. W. *J. Phys. Chem.* **1987**, *91*, 1996. Kamlet, M. J.; Taft, R. W. *Acta Chem. Scand.* **1986**, *B40*, 619.

(35) Eventova, I.; Nadler, E. B.; Frey, J.; Rappoport, Z. *J. Phys. Org. Chem.* **1994**, *7*, 28.

(36) (a) Benesi, H. A.; Hildebrand, J. H. *J. Am. Chem. Soc.* **1949**, *71*, 2703. (b) Mulliken, R. S.; Person, W. B. *Molecular Complexes*; Wiley: New York, 1969; Chapter 7, pp 81−90.

Table 8. 400 MHz ^{1}H NMR Chemical Shifts and Assignment of Enols 2b and 2c[a]

assignment	(*b*)	2b		2c
		$CDCl_3$[c]	DMSO-d_6[d]	DMSO-d_6[d]
β-*o*-*i*-Pr(Me)	(*a*)	0.03	0.09	−0.07
	(*d*)	0.93[e]	0.94	0.97
β-*o*-*i*-Pr(CH)	(*B*)	2.57[f]	2.74	2.65[f]
β-*o*-*i*-Pr(Me)	(*j*)	1.22[g]	1.23	1.29[d]
	(*k*)	1.30	1.29	1.29[d]
β-*o*-*i*-Pr(CH)	(*F*)	3.31	3.20[h]	3.42[f]
p-*i*-Pr(Me)	(*efgh*)	1.15[i]	1.14[i]	1.12[i]
p-*i*-Pr(CH)	(*CD*)	2.79[f]	2.79[f]	2.76[f]
β′-*o*-*i*-Pr(Me)	(*b*)	0.08	0.16	−0.03
	(*c*)	0.93[d]	0.91	0.87
β′-*o*-*i*-Pr(CH)	(*A*)	2.57[f]	2.65	2.65[f]
β′-*o*-*i*-Pr(Me)	(*i*)	1.20[g]	1.20	1.20
	(*l*)	1.21	1.32	1.33
β′-*o*-*i*-Pr(CH)	(*E*)	3.11	3.10	3.10
=CR		1.93[j]	1.80[j]	1.10[k]
β-Tip-H	(*I*)	6.74	6.72	6.68
	(*III*)	6.99	7.01	6.99
β′-Tip-H	(*II*)	6.80	6.75	6.73
	(*IV*)	7.05	6.98	6.98
OH		5.10	8.14	7.49

[a] All values in *δ* (ppm) relative to internal TMS standard. [b] The labeling parallels that in Figure 6. [c] At 245 K. [d] At 298 K. [e] One 2Me doublet. [f] One 2H septet. [g] dd. [h] Approximate value since the signal overlaps the water signal. [i] Integrates for 12H. [j] Me signal. [k] C-Me_3 signal.

Table 9. ^{13}C NMR Data for 2b and 2c in $CDCl_3$ at 298 K[a]

assignment	2b	2c	assignment	2b	2c
i-Pr-Me	22.42	22.54	*p*-*i*-Pr-CH	33.87	33.78
	22.49	22.99		33.97	33.88
	22.83	23.78	C_β	107.15	105.80
	23.89	23.95[b]	*m*-Tip-C	121.28	121.65
	23.96	24.17[c]		122.33	122.31
	23.99	24.87		122.59	122.44
	24.60	25.45		123.51	123.39
	24.69	26.11	*ipso*-Tip-C	132.17	134.46
	24.84			134.97	136.59
	25.01		*o*-Tip-C	148.23	147.37
	26.03			148.42	148.48
	26.29			148.80	149.48
o-*i*-Pr-CH	29.48	28.06		150.03	150.47
	30.03	28.90	*p*-Tip-C	147.07	146.81
	30.27	29.89		148.16	147.90
	30.53	29.93	C_α	151.04	159.43
			R	19.39[b]	
				29.53[b]	37.77[c]

[a] TMS as internal standard. [b] Me signal. [c] C-Me_3 signal.

Due to the stereodynamic process, the ^{1}H NMR spectrum of **2a** at rt in weak and in good hydrogen-bond-accepting solvents is broad and sharp, respectively. Addition of small amounts of DMSO-d_6 to a sample of **2a** in CCl_4 causes sharpening, and at ca. 10% DMSO-d_6 in CCl_4 the spectrum is as sharp as in pure DMSO-d_6. This sharpening parallels the steep increase of *δ*(OH) and decrease of $^3J_{HCOH}$ observed upon addition of DMSO-d_6 to CCl_4, suggesting that the **2a**/solvent association alters both the C=COH and the Tip_2C=C conformations.

Static and Dynamic Stereochemistry of 1-Me- and 1-t-Bu-Substituted 2,2-Ditipylethenols. The ^{1}H and ^{13}C NMR Spectra of Enols 2b and 2c at Slow Exchange. The ^{1}H and ^{13}C NMR spectra of 1-methyl (**2b**) and 1-*tert*-butyl-2,2-ditipylethenol (**2c**) measured under slow exchange conditions resemble that of **2a** and are consistent with a frozen propeller conformation on the NMR time scale. Consequently, the signals were assigned (Tables 8 and 9) by analogy to **2a**.

The two unusually high-field *i*-Pr-methyl doublets found in **2a** are even more shielded in **2b** and **2c**, reaching negative *δ* values in **2c** (Table 8). This remarkable upfield shift is attributed to the proximity of these methyls to the shielding zone of the adjacent tipyl rings. The increased bulk of the α-alkyl group apparently forces the already shielded methyls into an even more shielded environment. This may result from an increase in the Tip-C=C torsional angle analogous to that found in ethenols **1a**−**e**, but evidence for this is lacking. Second, as for **1a**−**e**, the *δ*(OH) values in DMSO-d_6 decrease with the increased bulk of the α-alkyl group. Consequently, in DMSO **2b** and **2c** adopt an *anti*-type conformation in which the OH is hydrogen bonded to one DMSO molecule.

Table 10. Coalescence Data for Tip_2C=C(OH)R at 400 MHz

	R	solvent	process	Δ*ν*, Hz	T_c, K	$\Delta G_c^{\ddagger}$ kcal mol^{-1}
2b	Me	DMSO-d_6	*β*-*o*-*i*-Pr-Me ⇌ *β*-*o*-*i*-Pr-Me	480.0[a]	355[e]	16.0
				116.0[b]	331[e]	15.8
			β-*o*-*i*-Pr-CH ⇌ *β*-*o*-*i*-Pr-CH	184.1	345[e]	16.2
			β-*m*-Tip-H ⇌ *β*-*m*-Tip-H	117.0	338.0	16.1
			β′-*o*-*i*-Pr-Me ⇌ *β′*-*o*-*i*-Pr-Me	416.1[c]	355[e]	16.1
				164.0[d]	331[e]	15.5
			β′-*o*-*i*-Pr-CH ⇌ *β′*-*o*-*i*-Pr-CH	180.0	345[e]	16.2
			β′-*m*-Tip-H ⇌ *β′*-*m*-Tip-H	90.3	338.0	16.3
2c	*t*-Bu	DMSO-d_6	*β*-*m*-Tip-H ⇌ *β*-*m*-Tip-H	124.0	345.2	16.4
			β′-*m*-Tip-H ⇌ *β′*-*m*-Tip-H	100.0	345.2	16.6

[a] *i*-Pr-Me's "a" and "k" in Table 8. [b] *i*-Pr-Me's "d" and " j" in Table 8. [c] *i*-Pr-Me's "b" and "i" in Table 8. [d] *i*-Pr-Me's "c" and "l" in Table 8. [e] ±5 K, see text.

The ^{13}C NMR spectra of **2b** and **2c** at rt displayed distinct signals for almost all their carbons (excluding accidental overlap). Assignment by analogy to **2a** was corroborated by gated decoupling. In both spectra only some of the peaks were slightly broad due to a dynamic process, and this was used to distinguish the *o*- from the *p*-*i*-Pr-*C*H and Tip-*C*'s since the latter remain sharp during the dynamic process. A comparison of *δ*(C_α) and *δ*(C_β) values of **2a-c** shows that, as for **1a**−**e**,[12b] increasing the bulk of the α-alkyl group deshields C_α and shields C_β. This is ascribed to the contribution of the canonical structure **8b** in which C_β is negatively charged, while C_α is positively charged, and hence they are shifted to a lower and a higher field, respectively. Elongation of the

$$\underset{\textbf{8a}}{Tip_2C{=}C(OH)R} \leftrightarrow \underset{\textbf{8b}}{Tip_2C^{-}{-}C(=O^{+}H)R}$$

C_α−C_β bond reduces the alkyl and the *β*-Tip group interaction, increasing the contribution of **8b** for the bulkier α-*t*-Bu group. Despite the increased bulk of the tipyl group, the differences in Δ*δ* values for the α-H → α-*t*-Bu change between dimesityl and ditipyl systems are relatively small: 0.6 ppm for C_β and 3.44 for C_α.

Dynamic NMR Spectra of 2b and 2c. When solutions of **2b** and **2c** in DMSO-d_6 were heated, all the *o*-*i*-Pr-Me, *o*-*i*-Pr-CH, and Tip-H signals first broadened and then coalesced. It was convenient to follow the dynamic process in the aromatic region where a lower number of signals interfere with the coalescence process (Table 10). Coalescence of the *i*-Pr-Me and -CH signals of **2b** was also followed, but the calculated rotational barriers should be treated with caution for four reasons. First, the measured T_c values are less accurate due to difficulties in distinguishing separate coalescence temperatures, due to the vicinity of pairs of coalescing signals. Second, since one *i*-Pr-CH signal overlaps the water signal present in the solvent, Δ*ν* is very approximate. Third,

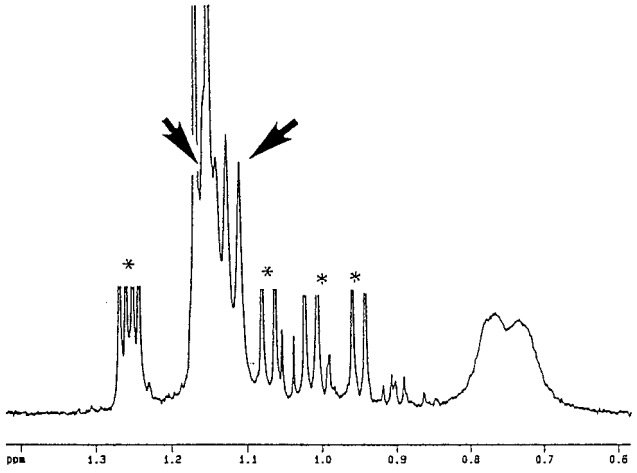

Figure 13. ^{1}H NMR spectrum of the *i*-Pr-Me region of **2b** at 420 K in DMSO-d_6. The impurity peaks (x) were truncated for clarity and belong to an oxidation product.

for the *i*-Pr-Me signals, identification of pairs of coalescing signals is based on the assumption that the process measured is a two-ring flip and not on an unequivocal experimental observation. Fourth, enols **2b** and **2c** undergo facile air oxidation upon heating to form polyalkylbenzofurans.[37] The ^{1}H NMR signals of the latter overlap the enols' signals and remain sharp over the whole temperature range, thus hampering an accurate determination of T_c. Oxidation of **2c** is so extensive that the coalescence was followed only in the aromatic region where the benzofuran signals are the least disturbing.

$\Delta G_c^{\ddagger}$(**2b**) = 16.0 ± 0.5 kcal mol^{-1} and $\Delta G_c^{\ddagger}$(**2c**) = 16.5 ± 0.1 kcal mol^{-1} (Table 10). These values are higher than those of the dimesityl analogues **1b** and **1e** as expected for the bulkier tipyl group. For both **2b** and **2c** the barriers measured for the exchange of magnetic sites at each ring are identical, suggesting a correlated motion of the two rings. However, supporting MM calculations are required to exclude occurrence of intermediate conformations in which the two rings rotate consecutively with identical barriers.[5]

If we consider only the *i*-Pr-CH and Tip-H signals, Table 5 shows that the observed site exchange can be attributed either to a [β,β']-two-ring flip, two succesive [β]- and [β']-one ring flip or to a simultaneous or succesive rotation of 180° by both rings. The observation of four averaged post-coalescence *o*-*i*-Pr-Me peaks in the ^{1}H NMR spectrum of **2b** at 420 K (Figure 13) excludes the two successive [β]- and [β']-one ring flip mechanism since, as discussed for the high energy rotational mechanism of **2a**, it should yield only three new peaks. In the two remaining possible mechanisms four post-coalescence peaks will appear but the average peaks generated in a two-ring flip ($a\bar{k}$ = 0.69, $d\bar{j}$ = 1.09, $b\bar{i}$ = 0.68, $c\bar{l}$ = 1.11 ppm) fit the experimental data (0.73, 0.77, 1.11, 1.14 ppm) better than those resulting from the nonhelicity reversal [β] and [β'] 180° rotation (aj = 0.67, dk = 1.13, bc = 0.53, il = 1.26 ppm). A temperature-dependent chemical shift may be responsible but over a 120 °C range δ(*p*-*i*-Pr-Me) shifted by only ≤0.1 ppm. Moreover, analogy between **2b** and **1b** suggests that the two-ring flip is the threshold enantiomerization mechanism. The coalescence data for the *p*-*i*-Pr-Me signals should enable us to distinguish these two possibilities (Table 5), but at 400 MHz these signals are not resolved. The coalescence data of the *o*-*i*-Pr-Me exclude the occurrence of an NMR-invisible, lower energy enantiomerization process such as a zero-ring flip. The average peaks ($a\bar{d}$ = 0.52, $k\bar{j}$ = 1.27, $b\bar{c}$ = 0.53, $i\bar{l}$ = 1.26 ppm) to be generated in this mechanism were not observed during the dynamic process, and hence, the proposed two-ring flip route is also the threshold enantiomerization mechanism of **2b**.

The threshold mechanism of **2c** was deduced by analogy to **2b**. From the coalescence of the Tip-H signals, $\Delta G_c^{\ddagger}$ = 16.5 ± 0.1 kcal mol^{-1}. The similar rotation barriers for the two-ring flip of **2b** and **2c** is in contrast with the 2 kcal mol^{-1} decrease in $\Delta G_c^{\ddagger}$ found for α-methyl- (**1b**) and α-*tert*-butyl-2,2-dimesitylethenols (**1e**). The linear correlation of the $\Delta G_c^{\ddagger}$ values for the two-ring flip process of **1a**−**e** with the torsional angle ϕ_2 suggests that the main effect of changing the α-alkyl group is steric. It is therefore puzzling why the decrease in $\Delta G_c^{\ddagger}$ values for the two-ring flip observed on replacing the α-H of **2a** by a methyl (**2b**) stops when the Me is replaced by a *t*-Bu group (**2c**), especially since the steric hindrance of the Tip_2C moiety exceeds that of Me_2C. It may be speculated that at a certain level of steric hindrance, which was reached in **2c**, $\Delta G_c^{\ddagger}$ start to increase again.

Summary. 2,2-Ditipylethenols **2a**−**c** exist in chiral propeller conformations in solution, and **2a** also in the solid. The peak assignment in solution and the ^{1}H and ^{13}C NMR spectra are consistent with the proposed conformation. **2a**−**c** undergo an enantiomerization processes on the NMR time scale involving a correlated rotation of the rings. The threshold mechanism for **2a** is a one-ring flip. The higher energy process is a two-ring flip mechanism. The rotation barrier for the one-ring flip is solvent-dependent. The rotational barriers ($\Delta G_c^{\ddagger}$) of **2a**−**c** are higher than those of **1a**, **1b**, and **1e** due to the increased bulk of the tipyl group. The threshold mechanism for **2b** and **2c** is a two-ring flip with $\Delta G_c^{\ddagger}$ values of 16.0 and 16.5 kcal mol^{-1}, respectively. $\Delta G_c^{\ddagger}$ of **2c** is higher than expected from the analogy with **2e**.

The conformation of the C=COH moiety of **2a** is solvent dependent. In good hydrogen-bond-accepting solvents (DMSO, DMF) it is *anti*-(peri)planar and the OH is hydrogen bonded to a solvent molecule, and in poor hydrogen-bond-accepting solvents it is *syn*-clinal having an OH···π stabilizing interaction with the ring cis to it. The *anti*-type conformer in DMSO−CCl_4 mixtures is associated with one DMSO molecule with K_{assoc} of 6.4, similar to the value for **1a**.

In summary, the changes in structure and behavior associated with the change β,β'-Mes_2 → β,β'-Tip_2 are in the expected direction, but are not very significant, except for the $\Delta G_c^{\ddagger}$ values.

Experimental Section

General Methods. Melting points were measured on a Thomas-Hoover apparatus and are uncorrected. UV spectra were measured on a Uvikon 930 spectrophotometer and FT infrared spectra on a Nicolet Impact 400 spectrometer. NMR spectra were recorded on Bruker WP 200 SY and Bruker AMX 400 pulsed FT spectrometers operating at 200.13 and 400.13 MHz and ^{1}H and 50.32 and 100.62 MHz for ^{13}C, respectively.

(37) This is reminiscent of the oxidation of 2,2-dimesitylethenols to the corresponding benzofurans, which were extensively investigated by Schmittel and co-workers (for represetative papers see: Schmittel, M.; Baumann, U. *Angew. Chem., Int. Ed. Engl.* **1990**, *29*, 541. Schmittel, M.; Röck, M. *Chem. Ber.* **1992**, *125*, 1611. Schmittel, M.; Heinze, J.; Trenkle, H. *J. Org. Chem.* **1995**, *60* , 2726) and of the oxidation of 2,2-ditipylethene-1,1-diol (Frey, J.; Rappoport, Z. *J. Am. Chem. Soc.* **1996**, *118*, 5182). These oxidations will be reported elsewhere.

MS were recorded on a MAT-311 mass spectrometer, and HRMS was conducted at the Mass Spectrometry Center at the Technion, Haifa, on a Finnigan Mat 711 apparatus. The X-ray diffraction data of the single crystals were measured with a PW 1100/20 Philips Four-Circle computer-controlled diffractomer. Mo Kα (λ = 0.710 69 Å) radiation with a graphite crystal monochromator in the incident beam was used. All crystallographic computing used the TEXSAN structure analysis software.

Solvents and Materials. Tetrahydrofuran (THF) was distilled from sodium benzophenone ketyl and ether from $LiAlH_4$. CCl_4 was dried by standing over $MgSO_4$ for 30 min and was then filtered. All purchased reagents were the best commercial samples and were used without purification. Polydeuterated solvents for NMR spectroscopy (Aldrich, DMF-d_7 was from Ferak, Berlin, Germany) were dried over 4 Å (DMSO-d_6 and DMF-d_7) or 3 Å (acetone-d_6 and acetonitrile-d_3) molecular sieves. THF-d_8 was kept in small portions in separate sealed ampules.

2,2-Bis(2,4,6-triisopropylphenyl)ethenol (2a). (a) Dehydration of 1,2-Bis(2,4,6-triisopropylphenyl)ethanediol. 1,2-Bis(2,4,6-triisopropylphenyl)ethanediol (50 mg, 1.1 mmol) was dissolved in AcOH (3 mL), concentrated HCl (0.5 mL) was added, and the mixture was refluxed for 3 h. Upon cooling, white crystals started to precipitate. AcOH (3 mL) was added, and the solution was heated until redissolution of the crystals. The solution was cooled slowly to room temperature, and the precipitated 2,2-bis(2,4,6-triisopropylphenyl)ethenol was collected (32 mg, 67%): mp 115−117 °C (lit.[16] mp 114−115 °C).

^{1}H NMR and ^{13}C NMR spectra are given in Tables 2 and 3. FTIR ν_{max} (Nujol): 3522 (s, OH) cm^{-1}. MS (EI) *m*/*z* (relative abundance, assignment): 448 (B, M). 405 (12, M − *i*-Pr), 387 (98, M − *i*-Pr − H_2O), 372 (12, M − *i*-Pr − Me − H_2O), 347 (17, M − 2 *i*-Pr − Me), 321 (14, M − *i*-Pr − 2 MeCH=CH_2), 279 (11, M − *i*-Pr − 3 MeCH=CH_2), 245 (15), 143 (15, $C_{11}H_{11}$), 131 (17, $C_{10}H_{11}$). HRMS: *m*/*z* 448.3729, requires 448.3705 calcd for $C_{32}H_{48}O$.

Crystal data: $C_{32}H_{48}O$. space group $P2_1/c$, a = 23.703(4) Å, b = 31.709(6) Å, c = 17.528(6) Å, β = 110.50(3), V = 12340(2) Å^3, Z = 16, ρ_{calc} = 0.97 g cm^{-3}, μ(CuKα) = 3.59 cm^{-1}, no. of unique reflections = 11201, no. of reflections with I ≥ 3σI = 8134, R = 0.099, R_ω = 0.130.

(b) Reduction of Bis(2,4,6-triisopropylphenyl)ketene. Bis(2,4,6-triisopropylphenyl)ketene[22] (230 mg, 0.5 mmol) was dissolved in dry THF (10 mL), and $LiAlH_4$ (70 mg, 1.9 mmol) was added. The resulting suspension was stirred at rt under argon for 1 h and cooled to 0 °C, and water (5 drops) was added to destroy unreacted $LiAlH_4$. $MgSO_4$ (50 mg) was added, the suspension was filtered, the solvent was evaporated to dryness, and the residual solid was recrystallized from hot AcOH, affording white crystals of bis(2,4,6-triisopropylphenyl)ethenol (137 mg, 59%), mp 115 °C. The $MgSO_4$ was dissolved in 3% aqueous HCl (10 mL) and the solution extracted with ether (4 × 25 mL). The combined organic phases were dried ($MgSO_4$), and the solvent was evaporated. Recrystallization of the residual solid from AcOH yielded an additional 73 mg of bis(2,4,6-triisopropylphenyl)ethenol (total yield 91%).

1,1-Bis(2,4,6-triisopropylphenyl)-1-propen-2-ol (2b). To a solution of bis(2,4,6-triisopropylphenyl)ketene (158 mg, 0.35 mmol) in dry ether (40 mL) was added MeLi (0.3 mL of a 1.4 M solution in ether) at rt under argon. After 10 min, 10% aqueous NH_4Cl (50 mL) was added. The organic phase was separated, washed with water (30 mL), and dried ($MgSO_4$), the solvent was evaporated, the residual light pink oil was dissolved in high-boiling petroleum ether, and upon standing at −18 °C very light pink crystals (90 mg, 56%), mp 141 °C, were formed.

^{1}H NMR and ^{13}C NMR spectra are given in Tables 8 and 9. IR ν_{max} (Nujol): 3510 (s, OH), 1630 (m, C=C) cm^{-1}. MS (EI) *m*/*z* (relative abundance, assignment): 462 (B, M), 420 (14, M − MeCH=CH_2), 419 (13, M − *i*-Pr), 377 (37, M − *i*-Pr − MeCH=CH_2), 335 (20, M − *i*-Pr − 2 MeCH=CH_2), 293 (10, M − *i*-Pr − 3 MeCH=CH_2), 251 (6, M − *i*-Pr − 4 MeCH=CH_2), 209 (5, M − *i*-Pr − 5 MeCH=CH_2), 131 (6, $C_{10}H_{11}$). HRMS: *m*/*z* 462.3892, requires 462.3861 calcd for $C_{33}H_{50}O$.

Anal. Calcd for $C_{32}H_{48}O$: C, 85.65; H, 10.89. Found: C, 85.88; H, 10.75.

1,1-Bis(2,4,6-triisopropylphenyl)-3,3-dimethyl-1-buten-2-ol (2c). To a solution of bis(2,4,6-triisopropylphenyl)ketene (253 mg, 0.57 mmol) in dry ether (15 mL) was added *t*-BuLi (0.6 mL of a 1 M solution in ether) at 0 °C in an argon atmosphere. After the mixture was allowed to stand at rt for 1.5 h, 10% aqueous NH_4Cl (30 mL) was added. Ether (30 mL) was added, the organic phase was separated, washed with water (30 mL), and dried ($MgSO_4$), and the solvent was evaporated to dryness, leaving a crude orange-red oil. Its ^{1}H NMR spectrum is nearly identical with that of the pure enol (**2c**), but four spots are apparent on silica TLC plates. The oil was dissolved in MeOH (10 mL), and an orange-pink precipitate (120 mg, 42%) was formed after 2 days at 4 °C.

^{1}H NMR and ^{13}C NMR spectra are given in Tables 8 and 9. FTIR ν_{max} (Nujol): 3566 (s, OH), 1584 (m, C=C) cm^{-1}.

Attempted isolation of an additional amount of **2c** from the mother liquor by silica gel chromatography (petroleum ether: ether 4:1 as eluent) yielded 2-*tert*-butyl-3-(2,4,6-triisopropylphenyl)-4,6-di(isopropyl)benzofuran (105 mg, 40%), mp 142 °C.

^{1}H NMR (400 MHz, $CDCl_3$) δ: 1.00 (6H, d, J = 6.8 Hz, *i*-Pr-Me), 1.05 (6H, d, J = 6.8 Hz, *i*-Pr-Me), 1.15 (6H, d, J = 6.8 Hz, *i*-Pr-Me), 1.16 (9H, s, *t*-Bu), 1.28 (6H, d, J = 6.9 Hz, *i*-Pr-Me), 1.30 (6H, d, J = 6.9 Hz, *i*-Pr-Me), 2.59 (1H, m, J = 6.8 Hz, *i*-Pr-CH), 2.86 (2H, m, J = 6.8 Hz, *i*-Pr-CH), 2.92 (1H, m, J = 6.9 Hz, *i*-Pr-CH), 2.99 (1H, m, J = 6.8 Hz, *i*-Pr-CH), 6.91 (1H, d, J = 1.5 Hz, benzofuran-H), 6.98 (2H, s, Tip-H), 7.15 (1H, d, J = 1.5 Hz, benzofuran-H). ^{13}C NMR (100.64 MHz, $CDCl_3$) δ: 24.15, 24.22, 24.31, 24.81, 25.24 (5 *i*-Pr-Me), 26.22 (*t*-Bu-Me), 29.15 (*t*-Bu-*C*Me$_3$), 30.24, 34.12, 34.18, 34.79 (4 *i*-Pr-CH), 104.94 (*C*=C-*t*-Bu), 110.96, 118.59, 120.45, 125.41, 129.36, 143.62, 144.70, 147.78, 148.39, 153.86, 158.49 (10 Tip-C + C=*C*-*t*-Bu). FTIR ν_{max} (Nujol): 1615, 1608 (m, C=C), 1417(s) cm^{-1}. MS (EI) *m*/*z* (relative abundance, assignment) 460 (B, M), 445 (59, M − Me), 403 (8, M − *t*-Bu), 387 (11, M − H − *t*-Bu − Me), 361 (6, M − *t*-Bu − MeCH=CH_2), 345 (7, M − H − 2*t*-Bu).

Anal. Calcd for $C_{33}H_{48}O$: C, 86.02; H, 10.50. Found: C, 86.18; H, 10.50.

Acknowledgment. We are indebted to the A. Gal Memorial Fund for support and to Prof. Silvio Biali for critical comments.

Supporting Information Available: Solvent effects, including the equations for calculating K_{assoc}, Figures S1−S7, Table S1, and tables of bond lengths and angles and a listing of positional and thermal parameters of **2a** (40 pages). This material is contained in libraries on microfiche, immediately follows this article in the microfilm version of the journal, and can be ordered from the ACS; see any current masthead page for ordering information.

JO971049Z